EDITORIAL BOARD

Annual Subscription

Pakistan: Rs 250 Foreign Countries: US$ 40 Overseas Air Mail Charges: US$ 10

The Journal is published bi-annually
In April and October

Published by:
Riaz Ahmad for Government College University, Lahore, Pakistan.

Printed at:
PRIME Publishers, Lahore, Pakistan.

CONTENTS

PK ISSN 0022- 2941; CODEN JNSMAC
Vol. 52; (2012) PP 01-07

THE EFFECTIVE MEASURING POINT OF THERMOLUMINESCENT DETECTOR AT THE BUILDUP REGIONS

M. S. AL-ARIF

Faculty of Science and Health, University of KOYA (UOK), Kurdistan-Iraq
*E-mail address: maan.safa@koyauniversity.org

(Received: April 04, 2013)

ABSTRACT: The present work provides accurate method for calculating the effective measuring point of the thermo luminescent (TLD) using the experimental measurements of the dose buildup ratio at the buildup region. A displacement correction factor is applied which shows to be varied with radiation dose stress ranging from maximum value at the interface region to zero value at the equilibrium region. The effective measuring point of the TLD accordingly is varied with the dose stress. The present method of calculation agrees with the theoretical trend and indicates that the effective measuring point is shifted toward the dose stress, and increases with increasing the differences in the atomic number of the interface media.

Keywords: TLD, effective measuring point, dose buildup ratio.

1. INTRODUCTION

In recent years a number of authors have reported problems when comparing photon depth-dose curves obtained experimentally and those obtained from detailed theoretical Monte Carlo simulations [1–4]. None seemed to fully explain the discrepancy between measurement and simulation. Some works reported significant differences in the measuring points between different detector systems [3].

In general when a measuring device is introduced into a radiation field, it tends to disturb the field. The output signal comes from the detector correlates to the integral dose over the detector thickness but practically we are interested in the dose in the medium at one measuring point. Different approaches where used to locate the effective measuring point in order to correlate the experimental measurement to one point inside the geometry of the detector. Methods that shift the effective point of measurements toward the source of radiation by a fixed amount are believed to be incorrect. The shift or the correction factor must be varied according to the dose perturbation stress. For example, at the interface region between dissimilar media, relatively sharp dose gradient near to the interface occur and gradually decreases with increasing distances and the displacement correction factor in the effective measuring point must be varied accordingly.

The present work aims to calculate the effective measuring point of the TLD for plane irradiation geometry using the experimental dose gradient at the interface for four interface media at two photon energies

2. MATERIAL AND METHOD

Consider a TLD disc of thickness, t, and the dose per unit thickness at depth, x, is Y(x). Assume the TLD disc is composing of two layers of $t/2$ thick each.

At distance far from the interface, the equilibrium dose achieved. The dose buildup ratio becomes constant, and the effective measuring point of the TLD is given by:

$$x_{eff} = \frac{t}{2} \quad (1)$$

At the buildup region, the effective measuring point must be shifted toward the radiation source because of the high dose stress near to the interface. The suggested formula for the effective measuring point is:

$$X_{eff} = S + \left[\frac{t}{2} - f\frac{t}{2}\right] \quad (2)$$

where ***S*** is the spacer thickness between the TLD and the interface, and ***f*** is the displacement correction factor, which is as:

$$f = f_1 - f_2 \quad (3)$$

Where; f_1 & f_2 represents the percentage dose contribution of the first layer of the TLD at the buildup region and at the equilibrium region respectively. f_1 & f_2 and are calculated as:

$$f_1 = \frac{\int_0^{t/2} Y(x).dx}{\int_0^{t} Y(x).dx} \times 100\% \quad (4)$$

$$f_2 = \frac{\int_0^{t/2} Y(x).dx}{\int_0^{t} Y(x).dx} \times 100\% \ = 50\% \quad (5)$$

The experimental measurements for different interfaces media indicate that the dose buildup ratio gradient is fitted by a negative power function of the following form:

$$Y(x) = a\,X^{-b} \quad (6)$$

Where; **a**, and **b** are constant depend on interface materials, and x is the depth in low atomic number medium.

The thickness of the TLD discs used in the present investigation is 3 μm. The integral dose of the two layers of the TLD disc accordingly is given by.

$$\therefore \quad Y = aX_1^{-b} + aX_2^{-b} \quad (7)$$

Where, X_1, and X_2, represent the midpoint thickness of the two layers of the TLD.

At the equilibrium region, the equilibrium dose buildup ratio is unity, therefore equation (6) become:

$$1.0 = a15^{-b}$$

$$\therefore \quad a = 15^{b} \quad (8)$$

At the interface region, we substitute for $a,\ S = 0,\ X_1 = 0.75,\ and\ X_2 = 2.25$ in equation (7) to gate:

$$b = \frac{\log Y}{3.255} \quad (9)$$

The constants, **a**, and **b** must be calculated for each interface media where **Y** represents the experimental reading of the TLD at the interface.

The dose buildup ratio of the two layers is given by:

$$\textit{First layer dose buildup ratio} \quad Y_{0.75+s} = a\,(0.75+s)^{-b} \quad (10)$$

$$\textit{Second layer dose buildup ratio} \quad Y_{2.25+s} = a\,(2.25+s)^{-b} \quad (11)$$

Therefore, equation (4) can be written as:

$$f_1 = \frac{Y_{0.75+s}}{Y_{0.75+s}+Y_{2.25+s}} \times 100\% \quad (12)$$

3. EXPERIMENTAL MEASUREMENTS

The irradiation geometry is shown in fig. 2. The radiation beam was directed perpendicularly to the surface of an approximately cylindrical phantom of Teflon material. The entrance field, symmetrically situated on the phantom surface, was 1.0 cm diameter and was defined by means of a special mask made of, lead, copper, aluminum, and Perspex.

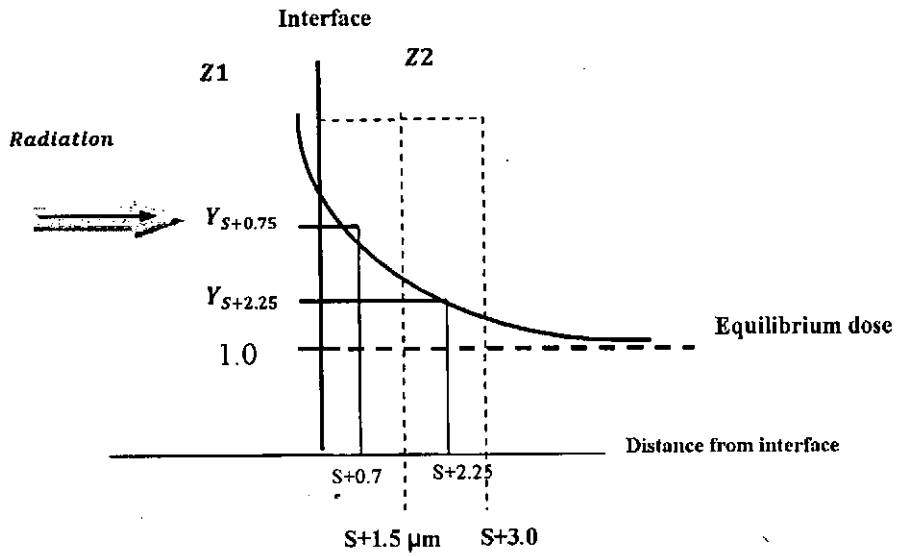

Fig. 1: Diagram to show the dose gradient from the interface. The TLD was assumed to consist of two parts. A midpoint of 0.75 µm and 2.25 µm plus the spacer thickness was used in the calculation of the dose for each layer.

The mask was arranged so that the material nearest to the detector was the material with the lowest k-edge. Since the transition region at low photon energies are extended only for a distance of about 15 microns from the interface, LiF/Teflon TLD's of 3 microns thick were manufactured and used in the present investigation at the

interface region. In practice, it is desirable to know to what degree the dose in low atomic number medium has been increased by the presence of higher atomic number medium. Thus rather than measure the absolute dose values, the dose build up ratio were determined. The thickness of each high atomic number material was chosen to be greater than the maximum electron range generated to ensure that the electronic equilibrium was established but sufficiently thin so that attenuation of the x-ray beam did not cause a significant quality change.

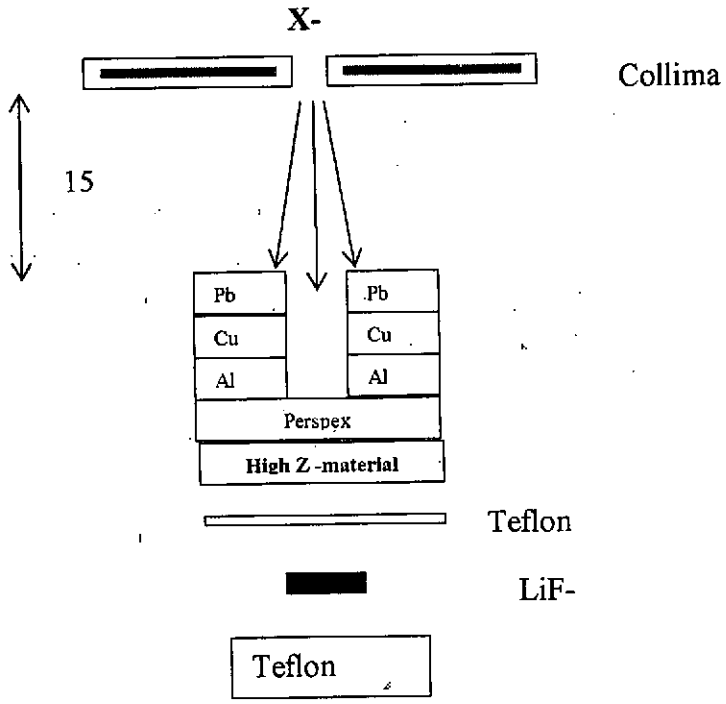

Fig. 2: The irradiation arrangement to measure the dose gradient at the vicinity of the interface between Teflon and higher atomic number medium.

4. RESULTS AND DISCUSSION

Table (1) shows the displacement correction factor, the measured dose buildup ratio, and the effective measuring point of the TLD at the interface region for two photon energies. It is shown that the displacement correction factor is varied with the dose stress ranging from maximum value at the interface to a zero value at the equilibrium region. Accordingly the effective measuring point of the TLD is shifted toward the radiation stress near to the interface and gradually decreases toward the equilibrium region at some distance from the interface. The present work indicates clearly that for the same spacer thickness, the dose stress increases with increasing the atomic number differences of the interface combination and increases with deceasing photon

energies. The present method of calculation for the effective measuring point agrees with the theoretical trend, reliable for similar geometries, and can also be used for depth dose measurements.

Table 1: The measured doses buildup ratio, the displacement correction factor, and calculated effective measuring point for different spacer thickness and different interface media at two photon energies.

(Al -Teflon) 80 KV b=0.094 a= 1.289

TLD Reading	Spacer thickness (μm)	Displacement correction factor (f)	X_{eff} (μm)
2.03	0	0.025	1.460
1.62	1	0.014	2.480
1.52	2	0.009	3.485
1.35	4	0.006	5.490
1.04	6	0.005	7.493
1.00	10	0.003	11.496

(Ti -Teflon) 80 KV b=0.261 a= 2.027

TLD Reading	Spacer thickness (μm)	Displacement correction factor (f)	X_{eff} (μm)
7.07	0	0.071	1.393
3.19	1	0.040	2.440
2.85	2	0.028	3.460
1.94	3	0.022	4.467
1.64	4	0.018	5.473
1.41	5	0.015	6.477
1.25	6	0.013	7.480
1.20	10	0.009	11.487

(Cu -Teflon) 80 KV b= 0.327 a= 2.424

TLD Reading	Spacer thickness (μm)	Displacement correction factor (f)	X_{eff} (μm)
11.5	0	0.088	1.360
5.21	1	0.050	2.420
2.82	2	0.035	3.450
2.48	3	0.027	4.460
1.71	6	0.016	7.475
1.22	10	0.010	11.485

(Sn-Teflon) 80 KV b= 0.387 a= 2.851

TLD Reading	Spacer thickness (μm)	Displacement correction factor (f)	X_{eff} (μm)
18.2	0	0.105	1.340
9.79	1	0.059	2.410
5.28	3	0.032	4.450
3.24	4	0.026	5.460
1.89	6	0.019	7.470
1.18	10	0.012	11.485

(Al-Teflon) 110 KV b=0.075 a= 1.227

TLD Reading	Spacer thickness (μm)	Displacement correction factor (f)	X_{eff} (μm)
1.75	0	0.021	1.470
1.62	1	0.012	2.480
1.42	2	0.008	3.488
1.31	3	0.006	4.490
1.29	4	0.005	5.492
1.15	6	0.004	7.493
1.00	10	0.002	11.496

(Ti-Teflon) 110 KV b= 0.228 a= 1.854

TLD Reading	Spacer thickness (μm)	Displacement correction factor (f)	X_{eff} (μm)
5.54	0	0.062	1.410
3.90	1	0.035	2.450
3.35	2	0.025	3.460
2.38	3	0.019	4.470
1.82	6	0.011	7.483
1.28	10	0.007	11.488

(Cu-Teflon) 110 KV b= 0.308 a=2.303

TLD Reading	Spacer thickness (μm)	Displacement correction factor (f)	X_{eff} (μm)
10.1	0	0.084	1.370
6.99	1	0.047	2.430
4.45	3	0.026	4.460
3.32	4	0.021	5.470
3.05	5	0.018	6.473
1.64	10	0.010	11.485

(Sn-Teflon) 110 KV b= 0.352 a= 2.594

TLD Reading	Spacer thickness (μm)	Displacement correction factor (f)	X_{eff} (μm)
14.0	0	0.095	1.360
4.49	1	0.054	2.420
2.10	2	0.045	3.430
1.45	3	0.029	4.460
1.13	4	0.024	5.464
1.02	6	0.017	7.470
1.00	10	0.011	11.487

REFERENCES

1. C. L. Hartmann Siantar, R. S. Walling, T. P. Daly, B. Faddegon, N. Albright, Paul Bergstrom, A. F. Bielajew, C. Chuang, D. Garrett, R. K. House, D. Knapp, D. J. Wieczorek and L. J. Verhey, Med. Phys., 28 (2001) 1322.
2. G. X. Ding, Med. Phys., 29 (2002) 2459.
3. W. Abdel-Rahman, J. P. Seuntjens, F. Verhaegen, F. Deblois, and E. B. Podgorsak, Med. Phys., 32 (2005) 286.
4. M. R. McEwen, I. Kawrakow, and C. K. Ross, Med. Phys., 35 (2008) 950.

PK ISSN 0022- 2941; CODEN JNSMAC
Vol. 52, (2012) PP 09-29

CHARACTERIZATION OF SOLID AEROSOLS RELATED TO FAISALABAD ENVIRONMENT AND THEIR PROBABLE SOURCES

M. A. K. SHAHID, K. HUSSAIN AND M. S. AWAN

Department of Physics, GC University, Faisalabad, Pakistan
E-mail Address: profkhan786@yahoo.com

(Received: November 30, 2011)

ABSTRACT: A comprehensive study was conducted to investigate the solid aerosols exposure, their effects and source identification in Faisalabad. For this purpose, Air samples were collected from specially selected zones representing Urban, Rural, industrial, residential cum commercial areas during day time from March 2006 to December 2006. The mass concentration was observed to be varying significantly during summer season. Urban and Industrial areas were found to be more polluted as compared to residential cum commercial areas in order of having higher concentrations of solid aerosols. Any significant variation regarding number concentration and size distribution of solid aerosols with respect to selected areas did not appear. Fine particles were accounted for 66.61% while coarse particles were accounted for 33.39%. The major identified sources of solid aerosols were

1. Long range sources such as sprays, earth soil eruption and industrial combustion (55.50%).

2. Short range sources such as crustal re-suspension, vehicular emissions and vegetation burning (30.35%).

3. The sources with mixed range were mainly of secondary nature. The maximum concentrations of solid aerosols were observed to be at industrial areas. A variety of particles with dominated silicon and soot particles (13.84%) were analyzed using SEM.

Keywords: Solid aerosols, trace elements, number concentration, major sources, Scanning Electron Microscopy.

1. INTRODUCTION

The present atmosphere is quite different from the natural atmosphere as it existed before the industrial revolution [1], in terms of its physico-chemical composition. If the natural atmosphere is considered to be "clean" as standard, then it means that one cannot find clean atmosphere anywhere in the world. This state of atmosphere gives rise to Air Pollution. Air pollution cannot be defined in a simple and easy way. One could claim that air pollution started with the beginning of burning of fuels for energy production and other purposes by humans. In other words, all manmade (anthropogenic) emissions into the air can be called air pollution because they alter the chemical composition of the natural atmosphere.

Historically these emissions had led to unforeseen consequences in the atmosphere. Pollution episode in London in December 1952 due to motor vehicle emissions causing urban smog resulted in rapid increase in mortality and morbidity rates and depletion of stratospheric ozone due to heterogeneous reactions of chloroflouro carbons with the ozone in 1970s are the examples of such consequences [2]. All such

type of emissions deteriorating human health and ecosystem are termed as air pollutants. Air pollutant is any substance emitted into the air from an anthropogenic source, i.e., either not the part of the natural atmosphere or is present in higher concentrations than the natural atmosphere and may cause a short term or long term adverse effect.

Atmospheric Solid Aerosols are now well recognized air pollutants contributing efficiently to the air pollution in modern era. The term "Aerosol" refers to an assembly of liquid or solid particles suspended in the gaseous medium. The particles in the aerosol are required to be stable in the gas long enough to be observed or measured. An aerosol is a two phase (or three phase) system consisting of both the particles (solid or liquid) and the gas in which they are suspended [3].

Aerosols are ubiquitous in air and often observable as smoke, dust and haze. They arise directly from emission of particles (Primary Aerosols) and from the conversion and condensation of certain gases to particles in the atmosphere (Secondary Aerosols) [4-5]. Solid Aerosols may also be classified with respect to possible sources of their generation. Natural Aerosols are generated naturally through volcanic eruptions, soil dust mobilization in deserts and production and decomposition of microorganisms/biological materials in the atmosphere. The other type is Anthropogenic Aerosols, as their name indicates are generated by anthropogenic or human activities like fuel combustion, biomass burning as well as agricultural, commercial and industrial activities [6].

According to a study conducted by WHO, Tehran, Calcutta and Bombay are found to be the most polluted cities in Asia [7-9]. Faisalabad in Pakistan is also pointed out to be as a highly polluted city in this report. The atmosphere of Faisalabad is getting polluted due to industrial growth, rapid urbanization and increasing rate of construction of commercial areas. This state of affairs inspired us to conduct a comprehensive study on air pollution in Faisalabad. So, firstly, Air samples were collected from specially selected zones in the city. Then the samples were analyzed using a number of techniques i.e., X-ray powder diffraction (XRPD), Scanning electron microscopy (SEM) and Atomic absorption spectrophotometry (AAS) for the comprehensive characterization and source identification of solid aerosols.

2. DATA ANALYSIS

2.1. MATERIALS

Faisalabad is the third largest city in Pakistan located in the Punjab with the population comprising of approximately 4 million citizens. The district is situated between 73° and 74o longitudes in East and 30° and 31.15° latitudes in North. Gujranwala and Sheikhupura districts are located in its north [10-12]. The climate of Faisalabad is hot and dry. Temperature ranges from 27oC to 50oC in summer and 6oC to 21oC in winter. Summer season lasts from the end of March to October while the winter season lasts from November to January. July and August are the months in which maximum rain fall occurs. The humidity in winter ranges from 46.9% in March to 54.5% in December while in summer it ranges from 57% in May to 79.5% in August [13].

Total (50) SPM samples were collected from different sites of Faisalabad city using Syntax Map Method and Simple Random Sampling (SRS) technique [14].

2.1.1 ZONE CLASSIFICATION

The city was divided into three zones, Zone I (Traffic/Industrial Zone), Zone II (Safe Zone), Zone II (Residential/Commercial Zone)

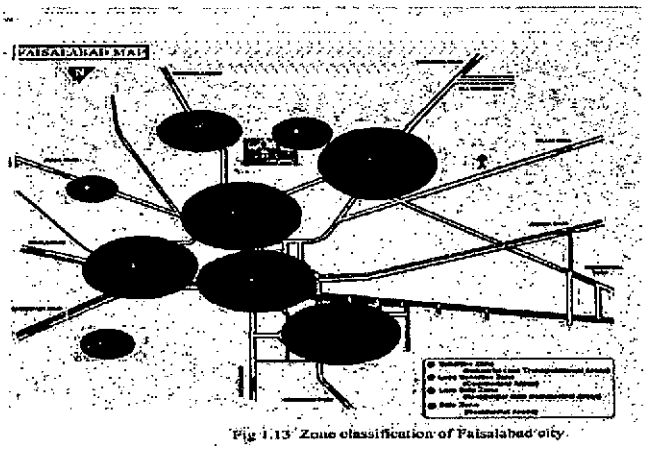

Fig 1.13 Zone classification of Faisalabad city

Fig.1: Zonal classification of Faisalabad city.

The detail is as follows (Table 1a & 1b).

Table 1a: Zone classification and sample numbers

Zone No.	Zone type	Sample codes	No. of samples	Sources of emission
1.	Industrial/Traffic Zone	2K05, 2K07, 2K08, 2K09, 2K10, 2K15, 2K18, 2K19, 2K20, 2K22, 2K23, 2K25, 2K27, 2K28, 2K29, 2K30, 2K33, 2K37, 2K38, 2K39, 2K40, 2K41, 2K42, 2K43, 2K44, 2K46, 2K47	27	Industrial/ Vehicular Emissions
2.	Suburb Zone	2K03,2K12,2K21	3	Residential/ Commercial Emissions
3.	Residential cum commercial zone	2K01,2K02,2K04,2K06,2K11,2K13,2K14,2K16,2K17,2K24,2K26,2K31,2K32,2K34,2K35,2K36,2K45,2K48,2K49,2K50	20	Background (Unpolluted Zone)

Most of the zone areas belong to city center while remaining were situated at (10-15) Km away from city center.

Table 1b: Area wise zone classification and grid selection using SYNTAX map method

Area category	*Well integrated roads*	*Poor integrated roads*
A_1	4	7
A_2	4	6
A_3	2	3

* Integrated radius = 5 km.

** Grid selection: (5 x 5) km.

2.1.2 Sample Collection and Sampling Mechanism

Sample collection was carried out using Kimoto High Volume air sampler. The high volume air sampler used to pump large volumes of air up to 2000 m^3 at a rate of 0.8 m^3/min. The filter used in a high volume air sampler was glass fiber filter having a collection efficiency of 99% for particles. Samples were collected for a period of 12 hours (720 minutes) at an average flow rate of (0.8 m^3/min). Particulate matter was trapped on each filter. Triplicate samples were collected from each place. A high flow rate (0.8 m^3/min) draw the air samples through a covered housing 20 x 25 cm rectangular glass fiber filters. The covered housing is necessary to protect the filter from precipitation and falling debris. Glass fiber filter was used because of their gradual head loss build up characteristics and non-hygroscopic properties. Contamination or damage to filter was avoided while inserting or removing them from the sampler. On removing from the sampler it was folded in such a way that surface

containing the deposits faced each other. The filter was weighed before and after sampling [15-17].

2.2. METHODS

2.2.1 Phase/compound analysis using XRPD

Phase/compound analysis of the Solid aerosols were carried out by employing an automated powder x-ray diffractometer (Rigaku model D/MAX-II A). The size and shape of solid aerosols were examined by SEM/TEM from sites of special scientific interests S3I under 80kv, at X1500, X2500 JEOL-1010 Model and elemental analysis was performed using Atomic Absorption Spectrophotometer (Varian 1475ABD) under controlled conditions.

The x-ray diffraction results reported in this study were obtained by running the diffractometer in the step-scan mode with the diffractometer conditions (Table 2).

Table 2.Diffractometer conditions used for analysis

Parameter used	Setting value
X-Radiation	Cuk_{α} (NI-Filtered)
X-Ray Tube Voltage and Current	35 KV & 20 m A
Divergent and Anti-scatter slits	1°
Receiving Slit	0.13 *mm*& 0.3 mm
Goniometer Scanning speed/step width	$1^{\circ}min^{-1}/0.02^{\circ}$
Rate meter time constant	1 sec.
Detector	Scintillation Counter
Start angle	65° (2Θ)
Stop angle	3° (2Θ)

The peak intensity, peak width at half maxima, d-values and Bragg angles were also noted using XRD x-y plotter during the step-scan mode. The relative intensities values were calculated for the above materials and presented in Table 3.

Table 3. Relative intensities of SPM minerals with KCl

Compound/Mineral	Relative intensity ($kI = I_i/I_{kcl}$)
Q	0.85
IL	0.20
T	0.32
G	0.83
CH	0.23
AL	0.36
C A	0.74
HM	0.89
HL	0.65

SP	0.49
MU	0.70
WS	0.16
R	0.27
AN	0.65

The suspended particulate matter (SPM) collected from randomly selected sites was strained in order to remove fibrous material. Samples were kept in bottles as such and were passed through two sieves for getting two parts of each sample having particle size less than 53 micrometer and less than 75 micrometer. All the samples were pressed gently in to aluminum/ glass holders before loading each of them on XRPD goniometer. The famous Henawalt and matrix flushing methods were employed for qualitative and quantitative analysis of the compounds present in solid aerosols.

3. RESULTS AND DISCUSSION

Environmental pollution due to solid aero sols is a major problem of the modern civilization. It is being increasingly felt that clean environment is as important as the basic necessities of life such as food, cloth and shelter. Environmental problems in Pakistan are growing at faster rate as compared with growth in the economy. It is evident from massive deforestation, salinity and water logging combined with progressive desertification, extinction of wild life, and degradation of landscape, water and soil resources. Faisalabad is one of the cities of Pakistan where situation is aggravating day by day. Rapid Urbanization, an Industrial expansion accompanying in the population growth are the major factors responsible for environmental pollution in general and air pollution in particular. The vehicle on city roads have been increased many folds and there are a great number of Industries in Faisalabad which are contributing heavily to the environmental pollution. Mean weight percentages of all the major phases identified in all the SPM samples are given in Table 4.

Table 4: Statistical analysis of major identified phases

Sample coding	Nature of the zone	Phases identified	Max.	Min.	Mean	S.D.	CV
2K95	R/C	IL	64.21	6.15	35.18	41.05	116.68
2K14	R/C	CA	64.52	1.92	33.22	44.26	133.23
2K15	I/T	G/T	70.58	4.22	37.41	46.90	125.36
2K47	I/T	Q	64.02	8.68	36.35	39.13	107.64
2K32	R/C	CH/CL	40.41	6.11	23.26	24.25	104.25
2K42	I/T	AL	34.20	6.51	20.36	19.57	99.11

XRPD studies carried out by matrix flushing method show that Gypsum and Talc is present in highest amount as indicated by their means (37.41) for each in almost all

the samples and Quartz (36.35), Illite (35.18), Calcite (33.22), Chlincore (23.26) and Albite (20.36) are also found in appreciable amount. Illite, Quartz, Calcite, Gypsum and Talc together were present in the samples with almost comparable mean weight percentages i.e. around 34% with their minimum and maximum values respectively 6.15% and 64.21%, 8.68% and 64.02%, 1.92% and 64.52%, and 4.22% and 70.58%. Chlorite/Chincholore and Albite were present in the samples with their mean weight percentages i.e, around 21% with their minimum and maximum values respectively 6.11% and 40.41% and 6.51% and 34.20%.The highest presence of Gypsum and Talc gives very interesting results as Faisalabad environment does not contain any source of these minerals, hence their origin lies at remote areas, the same is true for other such minerals. The detection of R, AN, HN, HL, SP, MU and WS as minor phases or the non-existence of these phases in polluted range is because of their larger size and not due to their existence below critical limits. These phases are of metallic, semi metallic and non-metallic nature, therefore their study becomes very important because they when combined with Oxygen Sulphate (SO4-2) and carbonate (Co3-2) radicals results the formation of complex compounds which shows the interaction of Industrial and Transportational dust, fumes with solid aero sols and pollute the environment, this aspect is evident from Gray (56%) / Black (30%) and Yellow (14%) color of most of the selected samples along with non-identified phases.

Micrographs taken from SEM showed that the size of the selected samples varies from 2µm to 93.3µm e.g. mixed composition of fine and coarse particles, which indicates the complexity of the Faisalabad. The size classification for four fractions PM (0.5-10) µm, PM (10-20) µm, PM (20-40)µm, PM >40 µm was carried out using sieve method and confirmed by SEM. PM (0.5-10) µm were found to be most abundant in the atmosphere of Faisalabad followed by PM (10-20) µm and PM (20-40)µm while coarse/giant particles PM>40µm showed lower concentration in 5 specially selected sites (S31 – S35) as shown in the table below:

Table 5: Size Distribution of the Solid Aerosols

Sample Code	0.5- 10µm %	10 - 20µm %	20 - 40µm %	> 40µm %
S^3I 1	78.12	15.62	6.25	-ND-
S^3I 2	60	20	20	-ND-
S^3I 3	65.00	16.66	10	23.34
S^3I 4	38.46	38.46	23.07	-ND-
S^3I 5	71.42	17.85	10.72	-ND-

Since majority of solid aerosols are in respirable mode and have anthropogenic origin, they may cause severe health hazards as a result of their inhalation. Some

micrographs show the combination of soot particles, fibers and silicates. Some may be derived from plant material and some with silicates of crystalline shapes. In short the interpretation of these micrographs have shown that silicate crystal and amorphous both (crustal origin) and soot particles (Industrial and transportational origin) are more prominent. Since the SEM used in this study was not equipped with EDX facility. The elemental analysis could not be carried out for confirmation of AAS results. For SEM results see in (Annex I) [18-19].

Wet Chemical analysis (WCA) of some samples was also carried out to check the co-relationship between identified trace elements by AAS and Phases of compound analysis by XRPD but nothing was found common between them except visibility reduction i.e. opacity or absorbance which shows semitransparent, semi opaque stack emission as the most basic effect of air pollution seen in the background of SEM micrographs, confirmed through QA/QC activity and Ringleman chart technique (EPA USA). The present study does not indicate any co-relationship between trace elements and identified phases in solid aerosols (Table 6 & 7) [20-25].

Table 6: Concentrations of Trace Elements (ppm)

Sample Coding	Nature of The Zone	Element Identified	Maximum Conc.	Minimum Conc.	Mean Conc.	SD	CV
			Range				
2K16	R/T	Ni	0.90	0.001	0.4505	0.6357	141.12
2K78	T/R	Cu	2.12	0.001	1.0605	1.498	141.25
2K11	R/C	Pb	0.082	0.001	0.0415	0.057	27.14

Table 7: Comparison of Identified Elements (Pollutant Macro Dynamic Equilibrium)

< or >or =PS	Cd	Cr	Ni	Cu	Zn	Pb
Violators >	54%	25%	29%	3%	Nill	24%
Followers =	3%	7%	Nill	Nill	Nill	4%
Better living standards <	43%	68%	71%	97%	100%	72%

Over All Net Effect, P1 > PS = 22. 5% (Pollutant Violators), P2 = PS = 2.4% (Pollutant Followers), P3 < PS = 75.2% (Better Living Standards)

PS* = primary standards

The Wet Chemical Analysis does not detect any compounds of Cd, Cr, Cu, Ni and Pb as shown below (Table 8) [26-28].

Table 8: Wet chemical analysis of solid aerosols

Oxide	Percent composition of Solid Aerosols

SiO_2	60.4800
Fe_2O_3	9.3000
TiO_2	9.3000
Al_2O_3	9.3000
CaO	7.8000
Na_2O	5.1600
K_2O	2.6666
Loss of Sample was observed	12.0200

Solid aerosols contribution towards rain acidification depends upon PH value, which gives us the proper identification of regions where acidic rains can take place. Keeping in view the PH value of solid aerosol samples, the acidic rain probability was calculated zone wise as given in table 10. Color of the samples and their PH values represents that the overall probability of acidic rain in the Faisalabad environment is only 20% as depicted in Table 9.

Table 9: Zone wise Probability of Acidic Rain

Zone	PH Value	Probability
Normal or acidic Zone (1)	7-8	49 %
Highly non acidic Zone (2)	8-9	42 %
Very Highly non acidic Zone (3)	9 & above	9 %

Table 10: Probability of Acidic Rain based on color and PH value

Color	Probability
Light Color (Acidic)	20%
Dark Color (Basic)	80%

The probability of acidic rain may however be completely ruled out in highly non acidic zone and Very highly non acidic zone (Table 9 and 10) because of the alkaline nature of solid aerosols which completely neutralizes the acidity of the atmosphere at present. Normal or acidic zone is safe presently but any change in industrial and transportational set up may give rise to a sensitive zone and make the pH values acidic.

Using the source marker table (11), [29-32], it was found that sources of solid aerosol pollution are 36% (Si rich), 27% (Al rich), making 63% primary origin while 9% (K/Ca/Na rich), 8%(Ni based) , 19% (Cu based), 0.72% (Pb based) making 37% secondary origin confirmed through XRPD compound analysis and AAS elemental analysis. This state of affairs also confirms the authenticity of Principal Component Analysis (PCA) and Cluster Analysis (CA) methods. The main sources of solid

aerosols are vehicular emissions (55.5%), metal industries (16.67%), coal combustion (13.68%), road dust (11.12%) and fly ash (2.72%) respectively.

Table 11: Source Markers for solid aerosols

Chemical Species	Possible Sources
Potassium (K^+)	Wood combustion, forest fires, prescribed burns, meat charbroiling
Sodium (Na^+) and Chloride (Cl^-)	Sea Salts
Nickel (Ni) and Vanadium (V)	Residual Oil combustion
Aluminium (Al), Silicon (Si), Calcium (Ca), Iron (Fe), Titanium (Ti)	Primarily from "soil" But also Smelters and Indicators (Ca, Fe)
Lead (Pb)	Vehicle exhaust/ Resuspended road dust
Bromine (Br)	Vehicle exhaust
Copper (Cu)	Smelter
Elemental Carbon (EC)	Fuel combustion and wild fires
Organic Carbon (OC)	Fuel combustion and wild fires
Hopanes and Steranes	Primarily mobile emissions
Polycycling Aromatic Hydrocarbon (PAHs)	Fuel combustion
Guaicols and Syringols	Biomass combustion

As for as fine to coarse ratio is concerned, it is calculated for Faisalabad, Pakistan and compared with the other similar studies conducted in Asia. It was found that average fine to coarse ratio i.e, 2.66 for Faisalabad is much greater than 0.68 for Nagpur, India, 0.78 for Hong Kong, China and 0.23 for Islamabad, Pakistan. Fine to Coarse ratio for Faisalabad environment showed very high figures as compared to other Asian cities. It was almost 4 times more than that of other similar studies as shown in Table 12 [33-34].

Table 12: Mixing ratio of fine to coarse Solid Aerosols

Sample Code	pm2.5/pm10
2K01	2.608696
2K02	0.368421
2K03	2.529412
2K04	0.5
2K05	3.678571
2K06	8.5
2K07	2.615385
2K08	1.366667
2K09	1.772727
Average	2.659986

These results show that the Faisalabad is much more polluted not only with in Pakistan but also within its neighbors like India and China. Fine to coarse ratio can also be used as an important indicator to infer PM2.5 concentration from existing PM10 monitoring network available from many air pollution network sponsored by

Government and Semi government agencies. It was also found that opacity is greater than luminosity which confirms the formation of Faisalabad Urban Boundary Layer (UBL) at (9m x 15m) probably related to Urban Canopy N-W high concentration maximum load of TSPM, (Sheikhpura to Jhang) S-E low concentration minimum load of TSPM, (Sahiwal/Okara to Sheikhupura) and converse which is due to Geographical and Geological setup of the selected sites as shown below (Table 13).

Table 13: Fall Rate (Tons/km2/month)/Wind Direction

Distance	N-W	S-E	N-E	S-W
3m	174	78	126	105
6m	148	64	108	102
9m	128	52	94	86
12m	106	38	72	72
15m	85	25	55	54

This may cause the shielding of Solar Radiation and hence decreases luminosity. Thus Traffic accident rates become more significant in evening (expansion in the canopy) than that of noon (contraction in the canopy) like rubber in spring. This state of affairs also indicates that the Solid Aerosol pollution at Faisalabad is positively contributing towards Global Warming not only because of Greenhouse gases but also due to shielding capability of Solid Aerosols. So, it is strongly recommended that immediate action must be taken to tackle with the pollution at Faisalabad. Wind direction effect, longitudinal and altitudinal effects on the concentration of solid aero sols shows that N – W direction has maximum load, hence it may be considered as potential danger region for acidic rain but due to Alkaline nature of Carbonates , bicarbonates of Ca, Na, K and Mg this may not happen. S – E direction has minimum load, which favours the nonoccurrence of acidic rain, so in near future the Faisalabad environment may be considered as safe environment from acidic rain point of view. Latitude and Altitude effects indicate that concentration of solid aerosols follow inverse square law, except some samples collected from sites of special scientific interests (S3I). This confirms the heterogeneous and complex culture of Faisalabad environment. No doubt these results are slightly disagreeable with international standards, but such type of information is very vital to know the geographical and geological conditions of concerned environment. Generally an increase in the concentration of dislocations will raise interfacial energy between the ice embryo and the nucleating particulate matter hence decreases its nucleability. A simple theoretical model was used to study this aspect. The most of the identified phases in the present study have large values of lattice misfit and they are poor nuclei particularly Quartz, Calcite and Albite which are poor nuclei they remain suspended in the atmosphere for long periods, depending upon their size hence supplement the poilution level of the

atmosphere as shown below (Table 14).

Table 14. Comparison of Cell Dimensions of Ice and Minerals Identified in Suspended Particulate Matter

Identified Phase	Crystal System	a (A°)	c (A°)	Basal Misfit % age	Prism Misfit % age
ICE	HEXAGONAL	4.490	7.338	-----	-----
QUARTZ	HEXAGONAL	4.913	5.450	9.2	17.8
ILLITE	MONOCLINIC	5.190	20.160	15.4	95.1
CHLINCORE	MONOCLINIC	5.320	14.290	18.3	56.1
CALCITE	HEXAGONAL	4.989	17.062	10.9	71.7
GYPSUM	MONOCLINIC	5.680	6.510	16.3	18.8
TALC	MONOCLINIC	5.287	18.964	17.5	88.0
ALBITE	TRICLINIC	8.144	7.160	81.0	41.7

In most of the samples identified phases occur as patches rather than single grain, so heterogeneity and aggregation of the Faisalabad environment is a dominating factor in our experimental findings. One possible explanation is that oxidation processes have converted the sulphides of identified phases into a soluble hydrous Sulphate which is confirmed by the Sulphate mineral as Gypsum detected in clay minerals by XRPD technique.

The other possible justification is that the presence of fly ash, road dust and pollens present in the Faisalabad environment have interlocked the identified phases into patches, the oval and irregular shapes of the majority of the samples also support our justification (Confirmation of Presence of Fibrous Material) as shown in the micrographs of SEM (Secondary Electron Microscopy). This state of affairs also confirms the stability of the Faisalabad environment. However further work is suggested to reconcile satisfactorily the techniques used in this study and their co-relationship with morphological structure studies. It is hoped that this study will be very useful towards the future environmental study programs related to Industrial areas cum commercial areas like Faisalabad [35-36].

4. CONCLUSIONS

The solid aerosols samples collected from various zones in Faisalabad show that they contain steadily the compounds namely Quartz, calcite and Albite as pollutants. The industrial zone has more amounts of quartz than that of residential zone. The source of these minerals is both local and remote The approximate size range of most of the dust particles is about 1 micron to 46 micron. Such particles remain suspended in the atmosphere for longer periods of times because they are not efficient nuclei of ice. The particles are therefore inhalable and can cause serious health hazards.

Some of other important conclusions are as follows:

- No chance of an acidic rain due to the presence of Calcite for the time being ~ 20%.
- Mix origin, 63% Primary (XRPD studies), 37% Secondary (AAS studies). Both have no co-relationship i.e, occurrence of physio-chemical reactions in the environment, (Physics and Chemistry of Faisalabad Environment has been changed).
- Source Marker method is as competent as Principal Component Analysis (PCA) and Cluster Analysis (CA) methods for source apportionment.
- Zone classification has no positive aspect all zones have dirty and clean patches i.e., mapping of Faisalabad is totally misfit with respect to Environment friendly.
- Most of the identified phases are poor ice nuclei i.e., have large lattice misfit, stay longer and supplement pollution, detection of Urban Boundary Layer (UBL) in urban canopy (9m x 15m) just equivalent to rubber spring.
- Fine to coarse ratio of solid aerosols is ~ 4 times than that of other similar studies which makes Faisalabad highly polluted area in the region, higher be the ratio, and higher be opacity, more be the global warming and converse [37-40].

ACKNOWLEDGEMENTS

The Authors are highly obliged to acknowledge the services of deputy director EPD, Director NIAB, Director NIBGE, Chairman, Department of Physics UET and Chairman Meteorological Cell Department of Crop Physiology, U. A. F, along with their technical teams for providing us technical assistance when and where needed. Their valuable suggestions, healthy discussions and positive criticism in getting this work completed in utmost ease and perfection.

REFERENCES

1. M. A. Awan, S. H. Ahmed, M. R. Aslam and I. A. Qazi, Iranica Journal of Energy & Environment, 2 (2) (2011) 128.
2. G. Capannelli, E. Castello, A. Comite, C. Costa and G. Mamolini, Journal of Electron Microscopy, 60(2) (2011) 117.
3. P. A. Baron and K. Willeke, Aerosol Fundamentals. 2nd Ed. New York: John Wiley and Sons, (2001) 45.
4. S. Woodward, J. Geophys. Res., 106 (D16) (2001) 18155.

5. G. S. Casuccio, S. F. Schlaegle, T. L. Lersch, G. P. Huffman, Y. Chen and N. Shah, Fuel Processing Technology, 85(6-7) (2004) 763.
6. S. P. Caudill, Statist. Med., 30 (2011) 515–521.
7. B. G. Bennett. J. G. Kretzschmar, G. G. Akland and H. W. Dekoning, Environ. Sci. Technol., 19 (1985) 298.
8. C. Gunawardana, A. Goonetilleke, P. Egodawatta, L. Dawes, A. Les and S. Kokot. Chemosphere, 87(2) (2012) 163.
9. H. M. Patterson and I. A. Gillette, J. Geophys. Res., 82 (1977) 2074.
10. M. Y. Hussain, M. Yousuf, Islam-ud-Din and M. Imran, Pak. J. Agri. Sci., 45(1) (2008) 112.
11. A. K. Sudheer and R. Rengarajan, Aerosol and Air Quality Research, 12 (2012) 923.
12. M. Ando and K. Tamara, Toxical Ind. Health., 7(5-6) (1991) 441.
13. L. Cheng, H. S. Sandhu, R. P. Angle and R. H. Myrick, J. Atmos. Environ., 32(22) (1998) 3835.
14. I. U. Chiemeka, International Journal of Physical Sciences, 5(4) (2010) 283.
15. N. Chong, K. Sivaramakrishnan, M. Wells and K. Jones, Electronic Journal of Environmental, Agricultural and Food Chemistry, 1(3) (2002) 145.
16. P. Chuaybamroong, C. Wu and D. A. Lundgren, Aerosol and Air Quality Research, 6(2) (2006) 213.
17. T. Nakamura, J. Power distillation, 3(2) (1988) 86.
18. M. Gentiliza, Vadjic and J. Hrsak, Environ. Monit. Assess, 11(2) (1988) 137.
19. K. Hussain, R. Riffat, A. Shaukat and M. A. Siddique, J. Advances in Atmospheric Science, 7(2) (1990) 178.
20. A. Boix, M. M. Jordan, T. Sanfelin and A. Justo, Atmospheric Environment, 27A (1994) 670.
21. H. Fu, M. Zhang, W. Li, J. Chen, L. Wang, X. Quan and W. Wang, Atmos. Chem. Phys. Discuss., 11 (2011) 20973.
22. C. Boni, E. Earuso, G. Lombardo and P. Redaelli, J. Aerosol. Sci., 19(7) (1988) 1271.
23. B. Davis, J. Aerosol. Sci., 18 (5) (1984) 469.
24. W. L. Faith and A. A. Atkisson, Inc. Canada, (1972) 457.
25. T. Fukasawa, M. Iwalsuki and S. P. Tillekeratnc, Environ. Sci. Technol., 17 (1984) 569.
26. A. V. Polissar, P. K. Hopke, W. C. Malm and J. F. Sisler, J. Aerosol.Sci., 26 (1995) 5589.
27. P. Roberts and J. Hallett, Q. J. Roy. Meteor. Soc., 94 (1968) 25.
28. W. Sahle, G. Sallsten and K. Thoren, J. Ann. Occup. Hyg., 34(1) (1990) 55.

29. J. C. Chow, J. Air Waste Manage. Assoc., 45 (1995) 320.

30. E. Sonja, B. Christoffer, N. Jere, K. Dan, M. Bostrom and H. Mikko, Energy Fuels, 25 (4) (2011) 1396.

31. M. A. K. Shahid, H. Khadim and S. A. Maryam, Journal of Basic & Applied Sciences, 8 (2012) 498.

32. S. P. Harrison, K. E. Kohfeld, C. Roelandt and T. Claquin, Earth-Science Reviews, 54 (2001) 43.

33. Z. Chowdhury, L. S. Hughes, L. G. Salmon and G. R. Cass, J. Geophys. Res-Atmo., 106(D22) (2001) 28597.

34. P. I. Jalava, R. O. Salonen, A. I. Halinen, P. Penttinen, A. S. Pennanen, M. Sillanpaa, E. Sandell, R. Hillamo and M. R. Hirvonen, Toxicology and Applied Pharmacology, 215 (2006) 341.

35. K. S. Johnson, B. Zuberi, L. T. Molina, M. J. Molina, M. J. Iedema, J. P. Cowin, D. J. Gaspar, C. Wang and A. Laskin, Atmospheric Chemistry and Physics Discussions, 5 (2005) 5585.

36. A. Tossavainen, J. Work Environ. Health, 5(4) (1979) 379.

37. Y. Mammane and K. E. Noll, Atmos. Environ., 19 (1985) 611.

38. M. W. Ashiq, Z. Chuanyan, N. Jian and M. Akhtar, Theoretical and Applied Climatology. 99(3-4) (2010) 239.

39. A. Srivastava, S. Gupta and V. K. Jain, Aerosol and Air Quality Research, 8(2) (2008) 188.

40. G. T. Wolff and P. E. Korsog, Atmos. Environ., 19 (1985) 1399.

ANNEXURE

DETAILS OF SITE SELECTION

KS - 01: (C/R): Faizabad Market start

KS - 02: (C): New Graveyard

KS - 03: (C/A): Outside UAF

KS - 04: (C/R): PMC Sargodha Road side

KS - 05: (I/C): Crescent Textile Mills

KS - 06: (R): Gulshan Colony

KS - 07: (T/R): Police Line outside

KS - 08: (R/T): near Allied Hospital & PMC side

KS - 09: (H): inside Allied Hospital

KS - 10: (R/T): Razabad outside

KS - 11: (R): Jinnah Colony

KS - 12: (C/A/H): Between Sahal Hospital and East Inn

KS - 13: (C): Shaheed-i-Millat Market

KS - 14: (R/C/T): Islamia College

KS - 15: (T): Jail Road

KS - 16: (R/T): Income Tax Office

KS - 17: (R: Model Town inside

KS - 18: (R/T): GC University

KS - 19: (R/T): between Ayub Research Colony &Niab

KS - 20: (R/T): Army Food Industries

KS - 21: (8 bazaars) Clock Tower

KS - 22: (T/R): Habib Bank building

KS - 23: (I/C: General Bus Stand

KS - 24: (R): Regency Arcade

KS - 25: (H): Saint Raphael Hospital

KS - 26: (C): Railway Goodams

KS - 27: (T/C): F.M.C. (Circular Road)

KS - 28: (C/I): Between Barah Market & Lyallpur Cotton Mill

KS -29: (C/T): Beneath Overhead Bridge

KS - 30: (C/T): Near Railway Station

KS - 31: (R): Tariq Abad inside

KS - 32: (C/R): between Nigebanpura&Mansoorabad

KS - 33: (C/I): outside General Bus Stand

KS - 34: (C/R): Rafhan Mill

KS - 35: (C): Flying Coach Stand

KS - 36: (C/R): Between DeegoResturant&SpinzerResturant

KS - 37: (I/R/A): Muhammad Abad, Sitana Road

KS - 38: (I/R/A): Overhead Bridge cinema side

KS - 39: (I/T/C): Overhead Bridge opposite cinema side

KS - 40: (T): Quaid-i-Azam Road

KS - 41: (I/T): Government College Samanabad

KS - 42: (T/C): New Big Graveyard, Jhang Road

KS - 43: (I/C) :Samundri Road

KS - 44: (I) : Iron Market

KS - 45: (R/A): Outside Peoples Colony-2

KS - 46: (I/C) : In between Peoples Colony-2 and Peoples Colony-1

KS - 47: (I/R/C): Jaranwala Road outside Kohinoor Mills

KS - 48: (R): Inside Kohinoor Mills

KS - 49: (R): Inside Madina Town

KS - 50: (I/R/C): Madina Town and Kohinoor Mills

AREA WISE ZONE CLASSIFICATION USING SYNTAX MAP METHOD

AREA-1

G_1:	(Zone-1)
INTERCITY HIGHWAYS:	
Sargodha Road	3.375 km
Sheikhupura Road	1.5 km
CITY ROADS:	
Bilal Road	0.30 km
Millat Road	1.75 km
Jail Road	2.875 km
Stadium Road	1 km
G_2:	
INTERCITY HIGHWAYS:	
Narwala Road	3 km
Jhang Road	2.25 km
CITY ROADS:	
Allamaiqbal Road	0.875 km
Government College Road	1 km
National Hospital Road	1.75 km

AREA-2

G_1:	(Zone-2)
INTERCITY HIGHWAYS:	
Summundri Road	3.25 km
CITY ROADS:	
Digkot Road	2.125 km
Samanabad Road	1.50 km
G_2:	
INTERCITY HIGHWAYS:	
Summundri Road	1 km
Sityana Road	2.05 km
Jaranwala Road	1.82 km
CITY ROADS:	
Railway Road	0.75 km
Circular Road	2 km
Kohinoor Road	0.50 km
Madina Town Road	0.50 km

AREA-3

G_1: (Zone-3)

INTERCITY HIGHWAY:

Jhumra Road 3 km

CITY ROAD:

Madina Town Road 1.375 km

G_2:

INTERCITY HIGHWAY:

Sheikhpura Road 0.75km

INTERCITY ROAD:

Jhumra Road 0.375 km

CITY ROADS:

Millat Road 3.25 km

The solid aerosols samples collected from various zones of Faisalabad were analysed and results are presented (Table 1-3) and the variation observed are displayed (Fig. 1-4).

In order to know which region had lighter SPM loadings than the others, Zone wise weight percentages of the identified minerals are given in Table 1 (Industrial Zone), Table2 (Suburb Zone) and Table 3 (Residential cum commercial Zone).

Table 1: Weight Percentage of Phases in SPM collected from Zone 1

Sample Code	R	IL	Q	CH/CL	AN	CA	AL	G/T	HM	HL	SP	MU	WS
2KO5	BDL	BDL	74.09	BDL	BDL	5.29	BDL	11.58	BDL	9.02	BDL	BDL	BDL
2KO7	BDL	BDL	72.41	BDL	5.42	15.84	BDL	6.34	BDL	BDL	BDL	BDL	BDL
2KO8	BDL	BDL	26.08	BDL	BDL	13.04	BDL	26.08	BDL	BDL	17.39	BDL	BDL
2KO9	BDL	BDL	76.36	BDL	BDL	23.63	BDL	17.03	12.52	16.05	BDL	BDL	BDL
2K10	BDL	BDL	41.15	BDL	BDL	BDL	BDL	29.91	12.52	BDL	BDL	BDL	BDL
2K15	BDL	BDL	29.42	BDL	BDL	BDL	BDL	70.58	BDL	BDL	BDL	BDL	BDL
2K18	BDL	BDL	18.38	BDL	BDL	BDL	16.72	BDL	BDL	39.40	13.78	16.72	BDL
2K19	BDL	66.2	15.60	14.38	BDL	3.72	BDL	BDL	BDL	BDL	BDL	BDL	BDL
2K20	BDL	BDL	38.36	BDL	BDL	18.32	37.67	5.62	BDL	BDL	BDL	BDL	BDL
2K22	BDL	59.62	5.72	17.03	BDL	5.69	11.68	15.43	BDL	BDL	BDL	BDL	BDL
2K23	BDL	37.09	BDL	30.70	BDL	10.00	BDL	4.84	BDL	BDL	BDL	BDL	BDL
2K25	BDL	29.56	BDL	29.32	BDL	12.65	19.42	BDL	BDL	BDL	BDL	BDL	BDL
2K27	BDL	56.68	13.34	15.15	7.06	BDL	BDL	BDL	BDL	BDL	BDL	BDL	BDL
2K28	BDL	34.97	27.82	BDL	BDL	3.72	7.74	BDL	BDL	BDL	BDL	BDL	BDL
2K29	BDL	63.63	14.98	BDL	BDL	8.24	5.82	7.34	BDL	BDL	BDL	BDL	BDL
2K30	BDL	BDL	9.86	14.14	BDL	7.56	23.54	10.21	BDL	BDL	BDL	BDL	BDL
2K33	BDL	8.28	BDL	35.28	BDL	BDL	22.53	8.54/ 25.35	BDL	BDL	BDL	BDL	BDL
2K37	BDL	38.09	BDL	33.12	BDL	BDL	21.15	7.61	BDL	BDL	BDL	BDL	BDL
2K38	BDL	33.63	BDL	29.24	BDL	BDL	18.67	8.09/ 10.34	BDL	BDL	BDL	BDL	BDL
2K39	BDL	54.4	4.87	19.92	BDL	10.27	BDL	5.51	BDL	BDL	BDL	BDL	BDL
2K40	BDL	59.73	20.37	15.58	BDL	BDL	BDL	4.32	31.52	BDL	BDL	BDL	BDL
2K41	BDL	36.83	10.94	33.09	BDL	6.80	12.31	BDL	BDL	BDL	BDL	BDL	BDL
2K42	BDL	6.15	14.48	BDL	BDL	13.63	34.20	BDL	19.6	BDL	BDL	BDL	BDL
2K43	BDL	48.28	11.35	6.11	BDL	5.77	28.00	BDL	BDL	BDL	BDL	BDL	BDL
2K44	BDL	37.03	8.71	BDL	BDL	8.47	20.57	19.60/ 5.60	BDL	BDL	BDL	BDL	BDL
2K46	BDL	45.82	10.77	16.33	BDL	8.09	BDL	7.22/ 11.73	BDL	BDL	BDL	BDL	BDL
2K47	BDL	9.87	64.02	BDL	BDL	14.17	11.93	BDL	BDL	BDL	BDL	BDL	BDL

Table 2: Weight Percentage of Phases in SPM collected from Zone 2

Sample Code	R	IL	Q	CH/CL	AN	CA	AL	G/T	HM	HL	SP	MU	WS
2KO3	BDL	BDL	24.42	BDL	BDL	21.78	BDL	19.84	BDL	BDL	BDL	BDL	33.82
2K12	15.96	BDL	25.92	BDL	BDL	BDL	BDL	32.03	6.89	BDL	19.84	BDL	BDL
2K21	BDL	35.48	26.34	21.18	BDL	17.00	BDL	BDL	BDL	BDL	BDL	BDL	BDL

Table 3: Weight Percentage of Phases in SPM collected from Zone 3

Sample Code	R	IL	Q	CH/CL	AN	CA	AL	G/T	HM	HL	SP	MU	WS
2KO1	BDL	BDL	66.80	BDL	5.31	23.23	BDL	BDL	BDL	BDL	BDL	BDL	5.31
2KO2	BDL	BDL	29.02	BDL	BDL	BDL	BDL	26.70	BDL	11.9	BDL	30.36	BDL
2KO4	33.66	BDL	16.99	BDL	BDL	15.06	BDL	17.88	5.79	BDL	BDL	10.60	BDL
2KO8	BDL	BDL	37.80	BDL	BDL	28.61	BDL	15.97	BDL	12.13	BDL	5.47	BDL
2K11	BDL	BDL	29.17	BDL	BDL	28.38	BDL	31.39	6.88	BDL	BDL	BDL	BDL
2K13	BDL	BDL	32.03	BDL	BDL	35.92	BDL	20.90	BDL	BDL	BDL	BDL	BDL
2K14	BDL	BDL	14.57	BDL	BDL	64.52	BDL	BDL	BDL	BDL	BDL	BDL	BDL
2K16	BDL	BDL	19.54	BDL	43.50	17.40	BDL	19.54	BDL	BDL	BDL	BDL	BDL
2K17	BDL	BDL	34.02	BDL	BDL	BDL	BDL	13.64	52.38	BDL	BDL	BDL	BDL
2K24	BDL	34.95	25.62	15.16	BDL	BDL	BDL	7.85	BDL	BDL	BDL	BDL	BDL
2K26	BDL	71.85	15.86	15.86	9.34	BDL	20.5	BDL	BDL	BDL	BDL	BDL	BDL
2K31	BDL	BDL	8.68	30.20	BDL	10.06	20.6	8.96/22.18	BDL	BDL	BDL	BDL	BDL
2K32	BDL	BDL	6.82	40.41	BDL	12.56	BDL	11.18/29.02	BDL	BDL	BDL	BDL	BDL
2K34	BDL	62	14.58	BDL	BDL	8.92	6.54	7.94	BDL	BDL	BDL	BDL	BDL
2K35	BDL	52.39	12.32	BDL	BDL	1.92	29.10	4.24	BDL	BDL	BDL	BDL	BDL
2K36	BDL	36.50	BDL	BDL	BDL	9.86	21.52	9.32/22.78	BDL	BDL	BDL	BDL	BDL
2K45	BDL	64.21	15.10	11.33	BDL	BDL	6.51	2.82	BDL	BDL	BDL	BDL	BDL
2K48	BDL	37.64	19.38	13.34	BDL	11.98	17.65	BDL	BDL	BDL	BDL	BDL	BDL
2K49	BDL	29.69	15.74	21.52	BDL	BDL	26.39	7.22	BDL	BDL	BDL	BDL	BDL
2K50	BDL	19.66	43.35	10.50	BDL	16.69	9.77	BDL	BDL	BDL	BDL	BDL	BDL

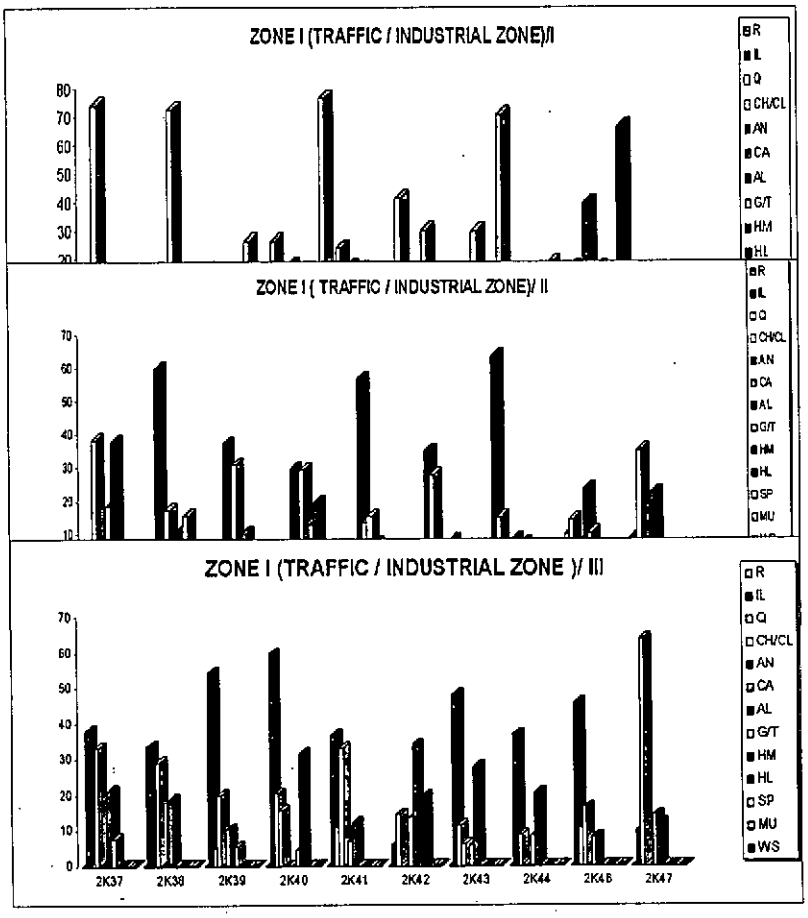

Figure 2: Weight Percentage of Phases Identified in SPM of Zone1 presented in three patches

Quartz was present in amounts ranging between 4.9 to 74.1 % in the SPM of Zone 1, 24.4 to 26.3 % of Zone 2 and 6.82 to 66.80 % of Zone 3, in about 18 samples of Zone 1 and Zone 3. The amount of quartz was about two to three times higher than for Zone 2. Illite was found to vary ranging between 6.2 to 63.6 % for Zone 1, 35.5 % for Zone 2 and 19.7 to 71.9 % for Zone 3. It was not detected in some samples. Calcite was present in amounts 3.72 to 23.63 % for Zone 1, 17.0% to 21.8 % for Zone 2 and 1.9 to 64.5 % for Zone 3. Figures 2 to 4 show the weight percentages of phases for Zone 1, Zone 2 and Zone 3 respectively.

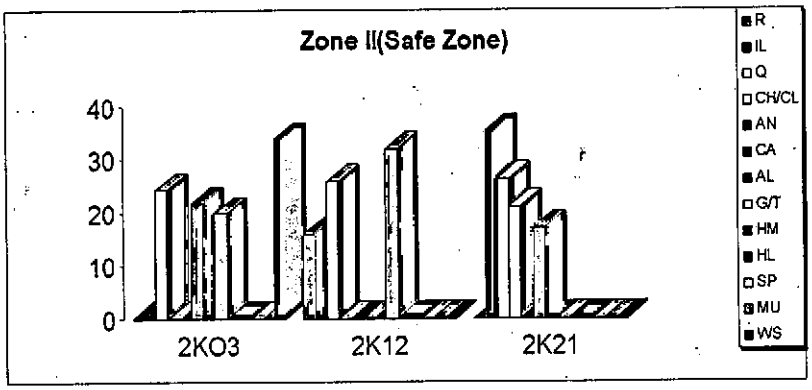

Fig. 3: Weight Percentage of Phases Identified in SPM of Zone 2

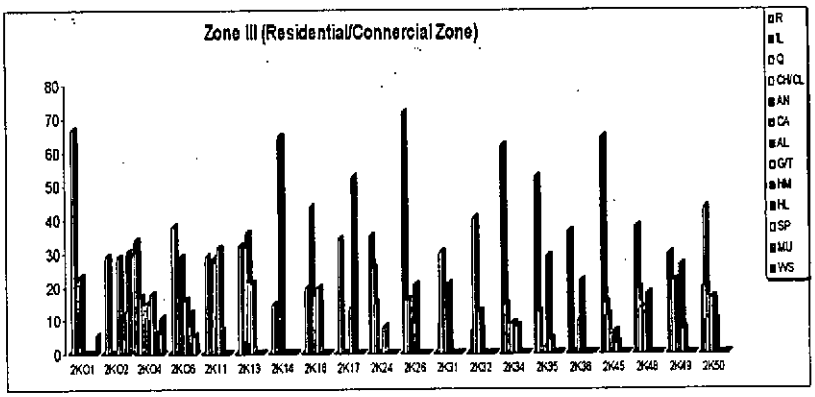

Fig. 4: Weight Percentage of Phases Identified in SPM of Zone 3

The results show that the most common minerals (clays/non-clays) identified in almost all SPM samples are Quartz, Illite and Calcite. Gypsum was identified in some 30 samples with amounts varying between 4.6 to 29.9 % for Zone 1, 19.8 to 2.0 % for Zone 2 and 2.0 to 31.4 % for Zone 3. The other phases detected in a few SPM samples were Albite, Talc, Hematite, Saponite, Mullite, Anorthite, Halite and Wustite.

The XRPD results do not show any dependence of the weight percentages of the identified phases on Zone characteristics. The occurrence of the phases in almost all

the Zones is found similar in weight percentages; such a result that the weight percentages of the major phases such as Quartz, Illite, etc were more in the industrial Zone than the other Zones is not found. Small and large amounts of these phases are identified for almost all Zones, and more specifically for Zone 1 and Zone 2. There would have been dirty and clean locations in the zones whether the latter were industrial or residential/commercial and consequently the amounts of phases were large and small. The dusty areas were near the roads from where the samples were collected. The results also do not show any dependence of weight percentages of phases on sample color or physical appearance.

The phase analysis of all the SPM samples showed presence of soil minerals and did not indicate presence of any compounds grown in the atmosphere through photosynthesis. It does not mean that such compounds did not grow photosynthetically in the atmosphere. The compounds grown photosynthetically were perhaps below the detection limit of the Diffractometer.

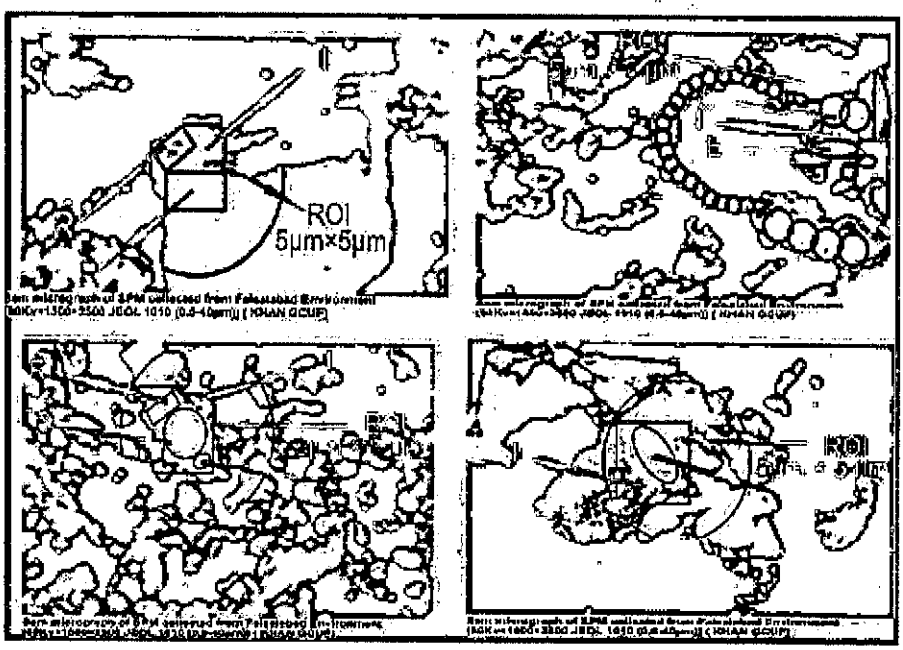

Fig. 5: Some SEM Micrographs showing Morphology of Solid Aerosols

PK ISSN 0022- 2941; CODEN JNSMAC
Vol. 52, (2012) PP 31-46

NITRIDING OF TITANIUM USING CAPACITIVELY COUPLED AC PLASMA

M. S. SHAH, U. IKHLAQ AND S. SALEEM

Department of Physics, Government College University Lahore, Pakistan
E-mail Address: ms_shah_sgd@yahoo.com

(Received: May 23, 2013)

ABSTRACT: Plasma nitriding of commercially pure titanium is carried out to improve the surface properties of titanium. Characterization of nitrogen plasma is carried out as a function of filling pressures for input power of 100 W. Nitriding is performed at 2 mbar and 3 mbar pressures for 2, 6, 10 and 14 h. The structural and compositional properties of nitrided specimens are investigated using x-ray diffractometer (XRD), optical micrography and micro hardness tester. Each sample exhibits an evidence of surface changes with substantial increase of surface hardness. XRD pattern confirmed the formation of hexagonal α_N-Ti and α-$TiN_{0.26}$ phases. Moreover, the discharge conditions at 2 mbar pressure for 14 h are favorable to nitride the surface of titanium.

Keywords: Gas-solid reactions; Plasma nitriding; Diffusion; X-ray diffraction; Surface properties

1. INTRODUCTION

Titanium and its alloys are used in a wide variety of industrial and commercial applications such as aerospace components, architecture, sports equipment, military hardware, medical implants, dental products, prosthetic devices and orthopedic applications due to their low density, low modulus of elasticity, strength to weight ratio, good corrosion resistance and biocompatibility [1]. These surface properties can be improved by exposing samples in nitrogen plasma environment. Nitriding of titanium and titanium alloys is used effectively for protection against wear. Titanium has a closed-packed hexagonal crystallite structure (HCP) known as α-Ti at room temperature. Nitrogen has a high solubility in α-Ti so it strengthens the surface layer significantly [2].

The nitrogen having atomic dimension much less than that of titanium can diffuse in to surface layer of the sample as interstitial solid solution. Plasma nitriding is promising technique owing to their potential use in modification of surface properties of various materials [3]. This technique has many advantages for thermo-chemical treatment such as control of the phase formation and the depth of nitrided layer. It requires short periods of nitriding time and is more versatile than other conventional methods [4]. Nitriding is primarily used to enhance fatigue strength, surface hardness, wear and corrosion resistance without affecting bulk properties of materials [5, 6].

Titanium nitrides have many applications in different industrial areas such as in cutting machineries, anticorrosive coatings, turbines, medical and biological materials

(especially artificial teeth and bones), structural materials in deep sea, microelectronics. Physical vapor deposition (PVD) techniques are widely used to deposit materials on a large variety of substrates [7]. The coatings by this technique are used in variety of applications such as optical, electrical, mechanical, chemical, and decorative purposes. Low temperature plasma nitriding is highly desirable to retain corrosion resistance and wear resistance. It can also produce nitrogen-enriched diffusion up to a significant depth and better adhesion in addition to create a hard surface layer [8].

Langmuir probe is one of the reliable diagnostic techniques widely used for measuring the plasma parameters such as electron temperature (eV) [9, 10], electron number density (cm^{-3}) [10, 11] and electron energy distribution function (EEDF) referred to as the Druyvestyn method [12, 13]. These parameters influence the production of active species by inelastic collisions, plasma reactions, and plasma surface interactions.
This paper reports the characterization of 50 Hz ac generated nitrogen plasma for nitriding of titanium and the effect of plasma parameters on the growth of nitrided thin film in terms of crystal structure, surface morphology and micro-hardness.

2. EXPERIMENTAL SETUP

Nitriding of titanium specimens is carried out in plasma generated between stainless steel electrodes each of 14 cm diameter and thickness of 2 cm. The electrodes assembly is arranged in a parallel plate (capacitive) configuration having inter-electrode spacing of 3 cm and housed in a stainless steel vacuum chamber of diameter and height of 32 cm shown in Fig. 1.

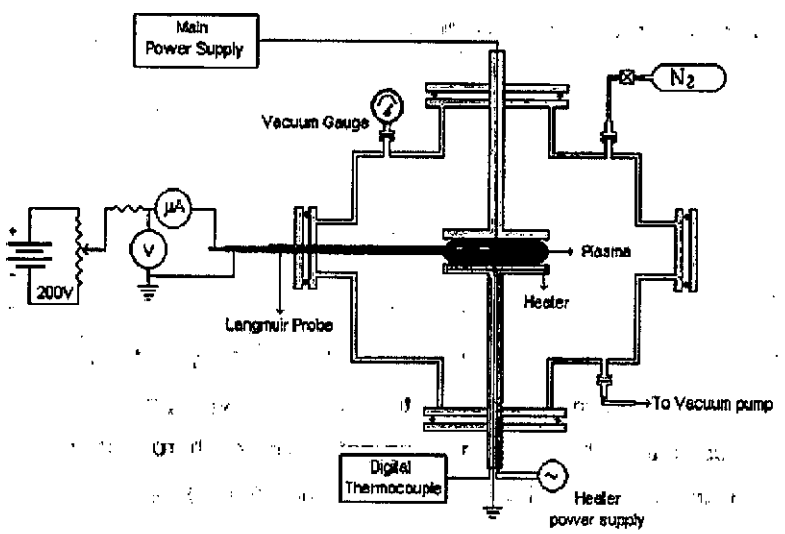

Fig. 1: Experimental set up of the plasma nitriding system.

The base pressure of the chamber is 1×10^{-2} mbar by using rotary pump and gas pressure is monitored using capsule type vacuum gauge of 0–25 mbar. An input power is applied to the top electrode using step-up transformer through an inductive load which limits the current during discharge. The specimens are placed on bottom electrode, which is grounded. The inlet and outlet valves are adjusted so as to maintain the required pressure in the chamber. The temperature of samples is monitored by thermocouple and maintained at 300°C. Nitrogen plasma is generated in abnormal glow regime. Langmuir probe I-V characteristics are recorded by varying pressure from 2 mbar and 3 mbar at constant power for DC bias voltages swept from -100 V to +100 V. It is observed that energetic species are produced at 2 mbar and 3 mbar pressures [5] which are selected after diagnosing the plasma and on the basis of previous studies. Therefore, only two pressures are used to nitride the surface of titanium. After nitriding the samples are cooled down in vacuum chamber in nitrogen atmosphere for 1 h.

Specimens of titanium ($9\times9\times3mm^3$) are mechanically polished with $\pm0.05mm$ dimensional accuracy using SiC abrasive paper on Stuers Knuth-Rotor-3 polishing machine, to a mirror finish, and then cleaned ultrasonically for 30 minutes with water. A Philips X' Pert PRO Panalytical x-ray diffractometer is used for analysis of nitrided titanium specimens which is operated at voltage of 40 kV and current of 40 mA for Cu $K\alpha_1$ radiation (λ = 1.540598 Å) source. Topography and layer thickness are investigated using Olympus CK 40M-CP (Japan) optical microscope. The microscope is attached with the Olympus Camedia C-5060 digital compact high revolution camera. The modified thin layer of the nitrided samples is examined at 50x magnification and measured with attached micrometer. Surface hardness of untreated and treated samples is measured using Wilson Wolpert 401 MVD™ Vickers micro hardness tester.

3. RESULTS AND DISCUSSION

3.1. Plasma generation reactions

Plasma consists of low and high energy nitrogen atoms or ions or electrons. In this plasma, the electrons are usually much more energetic than ions. These electrons play significant role in different chemical reactions, thereby interacting with nitrogen and titanium and excite the species through inelastic collision. These species can also absorb in the surface of titanium [8]. These atoms and radicals from the plasma can also react with species already adsorbed on the surface to form compound and release energy as a heat which would raise surface temperature. With the increase of

surface local temperature, nitrogen atoms and ions can overcome chemical barriers and diffuse into the substrate.

Nitrogen diffuses into the titanium forming interstitial solution of nitrogen in the hexagonal closed packed $\alpha-$Ti phase. The surface layer formed is called diffusion zone (α_N) [2]. This process can continue as long as the $\alpha-$Ti matrix can dissolve nitrogen at the nitrogen medium/solid interface (where the nitrogen concentration is the highest). Dissolved nitrogen reacts at the interface and leads to the formation of a new phase $TiN_{0.26}$ [2, 14]. Experiments [15-16] and theories [17] have demonstrated that kinetic energy of impinging ions and neutrals can enhance adatom mobility which is beneficial for surface diffusion, collision mixing and chemical reaction. This improves the surface morphology and decrease the defect density.

3.2. Effect of pressure

Fig. 2 shows the EEDF as a function of electron energy for 2 mbar and 3 mbar filling pressure of nitrogen which is determined by the expression [12, 13],

$$f_E(V) = \frac{4}{Ae}\left(\frac{m_e(V_p - V)}{2e}\right)^{1/2} d^2 I_{se}(V) / dV^2 \qquad (1)$$

where $f_E(V)$ is the electron energy distribution as a function of probe voltage (V), V_p plasma potential, A the probe area, I_{se} the electron saturation current, e and m are the electronic charge and mass. Electron energy decreases with pressure with lower tail energy, which is also reported by other researchers [18, 19].

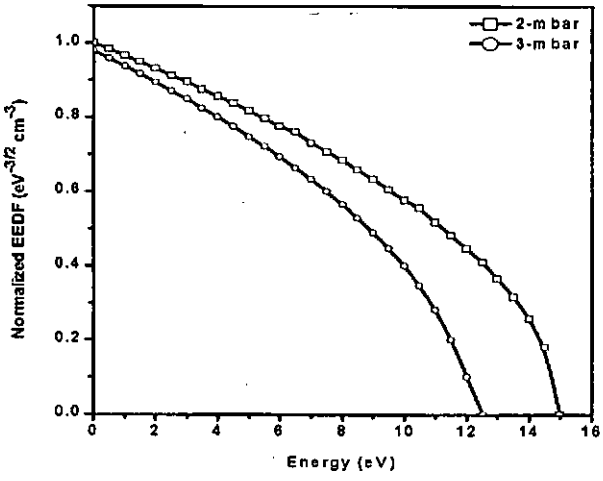

Fig. 2: Variation of electron energy distribution function (EEDF) as a function of energy for 2 mbar and 3 mbar filling pressure.

Fig. 3 shows electron temperature and electron density as a function of filling pressure. It is found that the electron temperature and density fall with increase of filling pressure in nitrogen plasma which is due to the increase in number of collisions between electrons and plasma species [10]. This increase in collisions is in turn, related to the partial pressure of the gas in the reaction chamber. The surface of titanium metal is very reactive to nitrogen. Atoms or ions in the plasma get higher energy which would bombard the surface. These energetic ions clean the surface and raise the temperature of the surface. This enhances the incorporation rate of reactive atoms into the surface. [20].

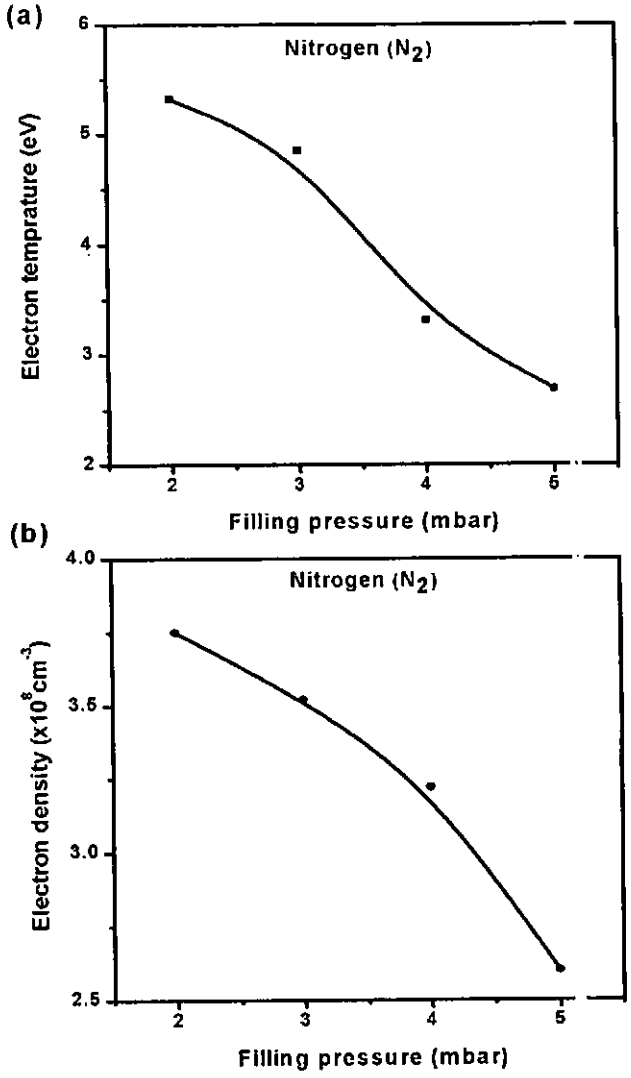

Fig. 3: Variation of electron temperature and density as a function of filling pressure of nitrogen.

3.3. X-ray diffraction analysis

Fig. 4 presents the XRD spectra of un-exposed and nitrided specimens at 2 mbar and 3 mbar pressure for different time durations. The un-exposed specimen has diffraction peaks corresponding to planes of reflections Ti (100), Ti (002) and Ti (101) confirming the closed-packed hexagonal (HCP) structure of alpha-titanium (α-Ti).

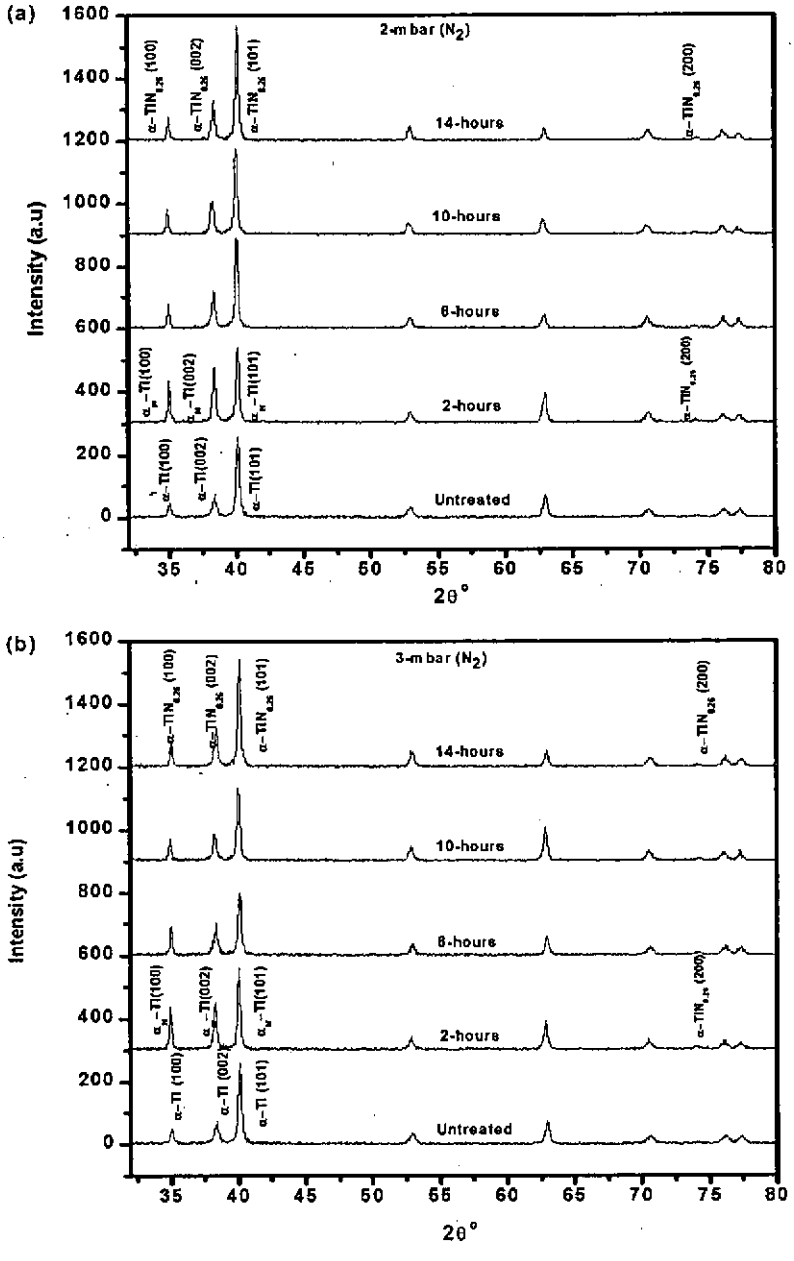

Fig. 4: The x-ray diffraction patterns of titanium specimens for different processing time at (a) 2 mbar filling pressure (b) 3 mbar filling pressure.

Fig. 5 shows the peaks of unexposed and exposed titanium for smaller range of angle in order to show the changes at 2 mbar and 3 mbar pressures for different time durations. Shift and broadening of peaks are observed at both pressures for different time durations owing to the diffusion or incorporation of nitrogen in titanium matrix.

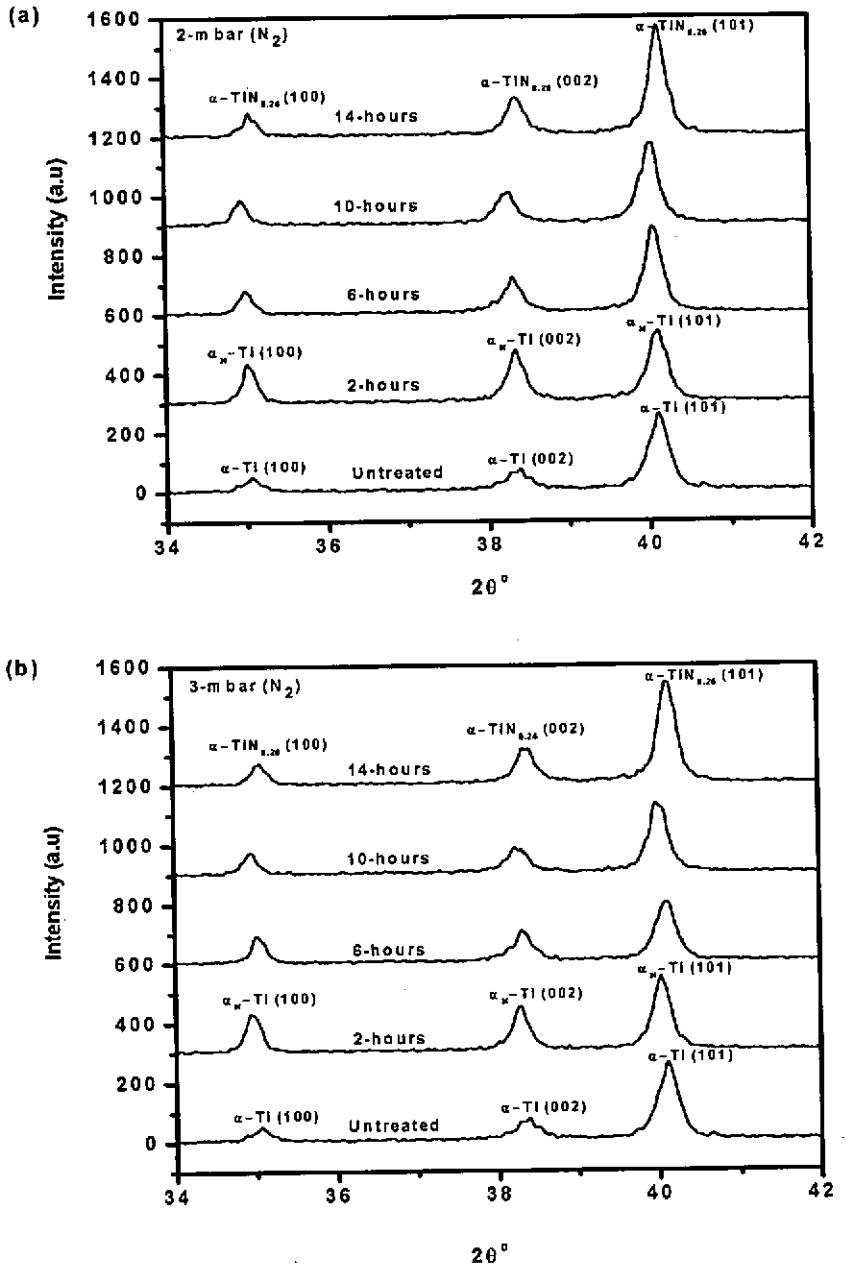

Fig. 5: Magnified XRD spectra of (100), (002) and (101) peaks of titanium and TiN for different processing time at filling pressures of (a) 2 mbar and (b) 3 mbar.

With the increase of time, the intensity of α-Ti phase increases at both pressures by the diffusion of nitrogen. Additionally, at $2\theta \approx 74.10^{\circ}$ a small and broad diffraction

peak of (200) reflection is observed at both pressures for different treatment time durations.

Fig. 6 shows the crystallite size of (101) reflection plane as a function of nitriding time which is calculated from Scherrer's formula [22],

$$Crystallite\ size = \frac{K\lambda}{FWHM\cos\theta} \tag{2}$$

Where K is a constant having value of about 1 and Full width at half maxima ($FWHM$) is the broadening of diffraction line measured. It is found that the crystallite size increases at 2 mbar filling pressure for 2 h, 10 h and 14 h due to the increase of nitrogen incorporation due to the increased adatom mobility. These incorporated ions produce stresses in the top surface layer. The decrease in crystallite size is observed at 6 h, which is due to the diffusion of nitrogen atoms or ions resulting in internal stresses [23]. This also related to the growth of thin film [24]. However, at 3 mbar pressure, the crystallite size increases at 2 h, whereas it decreases after 2 h and almost remains the same for the other durations of treatment time.

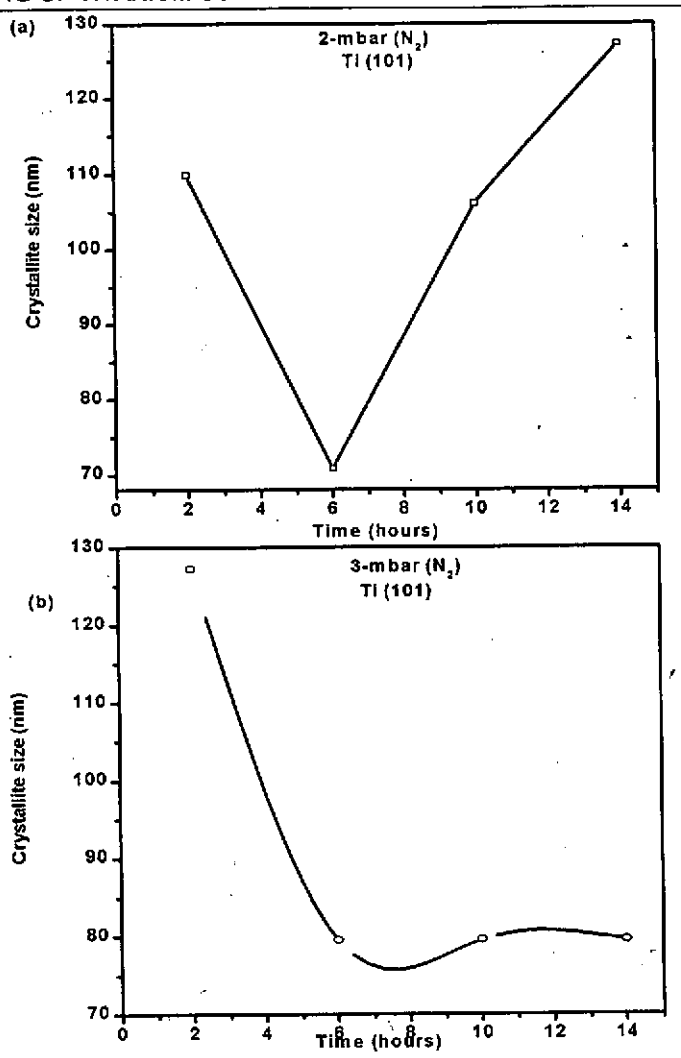

Fig. 6: Variation of crystallite size as a function of treatment time of Ti (101) reflection plane for pressure of (a) 2 mbar and (b) 3 mbar.

Fig. 7 shows the intensity of diffraction peak of (101) reflection plane as a function of treatment time observed from XRD spectra. Significant change in intensity and full width at half maximum (FWHM) of diffraction peaks compared with substrate is found at both pressures during the different nitriding time durations, showing the improvement in crystallinity. This increase in intensity indicates the improvement in the crystallinity which may be related to the presence of nitrogen contents in the samples [24, 25].

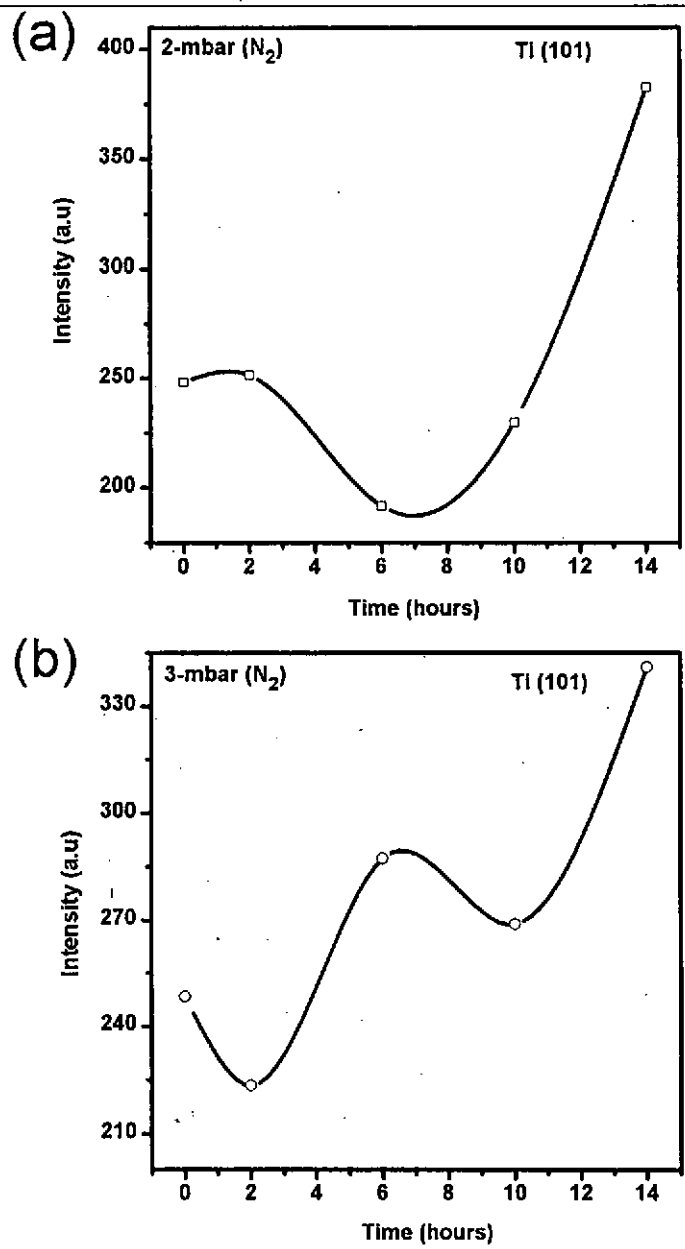

Fig. 7: Variation of intensity as a function of treatment time for pressure of (a) 2 mbar and (b) 3 mbar.

As pressure increases, the intensity of (101) reflection decreases as compared with the intensity at 2 mbar pressure for 14 h, causing the degradation of crystallinity [26]. Because the formation of more densely nitrided layer at higher pressure hinders the atoms or ions from further diffusion and leads to lower thickness which is due to the reduction of nitrogen vacancies with the increase of treatment time [24].

3.4. Optical morphology

Fig. 8 shows the topography of un-exposed and exposed specimen at 2 mbar and 3 mbar pressures for 14 h of processing time. Micrographs show that a layer of the film is deposited on the surface of substrate with time and surface layer seems to be smooth. However, the Ti-substrate processed by the nitrogen plasma in the present study has luminous gold-like appearance. Based on the optical micrographs, morphological behavior can be divided into two steps. The first step is the growth of an titanium nitride layer (α-Ti), which has low friction coefficient [21]. During second step, break down of the nitride layer produces fragments which may increase the friction coefficient [21].

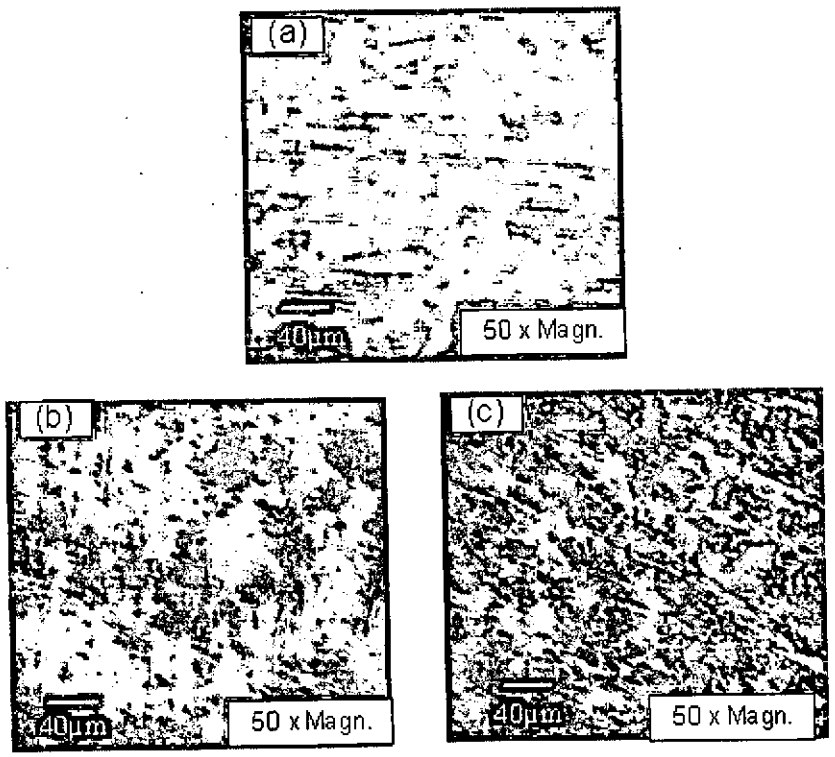

Fig. 8: Optical micrographs of specimen (a) untreated (b) treated at 2 mbar pressure for 14 h (c) treated at 3 mbar for 14 h.

Fig. 9 shows the cross-sectional optical micrographs of nitrided samples with different nitriding time durations (2, 6, 10 and 14 h) at 2 mbar and 3 mbar pressures. Picture evidence clearly indicates that a thin modified surface layer is formed by the diffusion of nitrogen in the titanium matrix. The thickness of modified surface layer as a function of nitriding time is shown in Fig. 10. It is inferred that the nitrided surface layer thickness increases with the increase of treatment time durations and decreases with

increasing pressure [25]. Further increase of nitriding time along with the high dose of nitrogen may result in the increase of surface roughness of substrate [26].

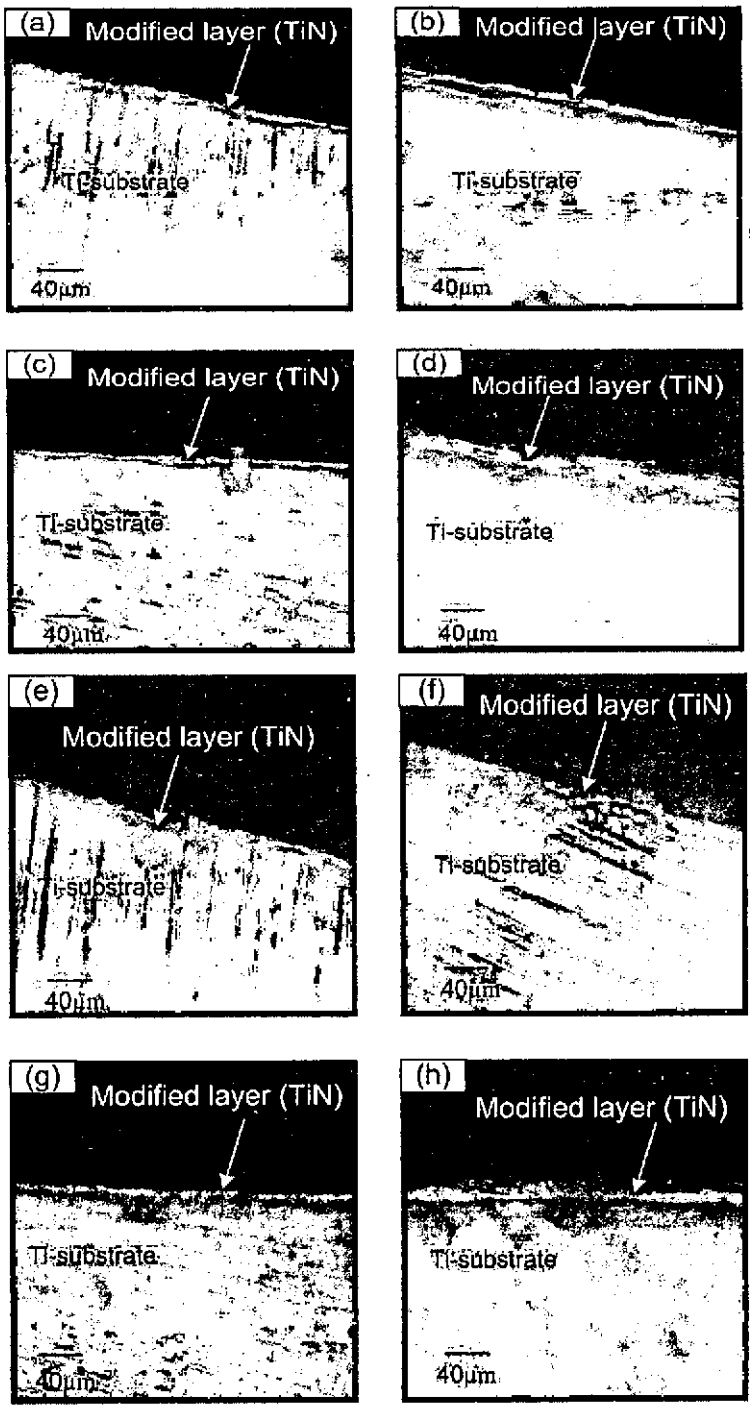

Fig. 9: Cross-sectional optical macrographs of specimen treated at (I) 2 mbar pressure for (a) 2 h (b) 6 h (c) 10 h (d) 14 h. (II) 3 mbar pressure for (e) 2 h (f) 6 h (g) 10 h (h) 14 h.

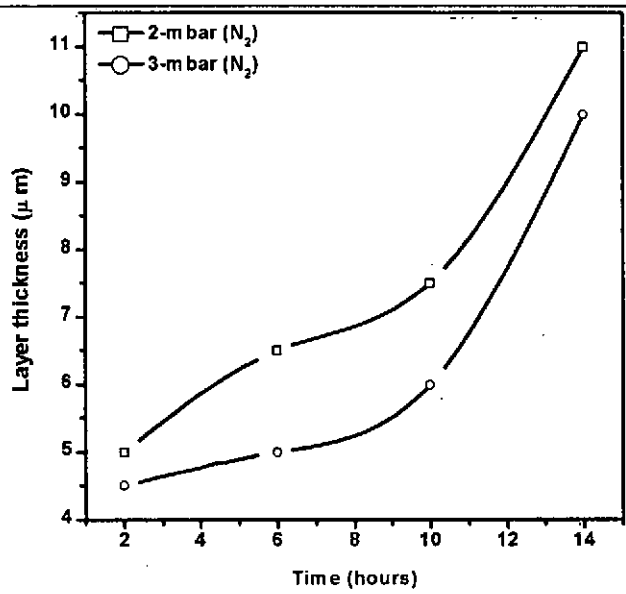

Fig. 10: Variation of modified surface layer thickness as a function of processing time at filling pressures of (a) 2 mbar and (b) 3 mbar.

3.5. Surface hardness measurements

Fig. 11 shows the surface hardness measured as a function of different imposed loads (0.01, 0.025, 0.05, 0.1, 0.2, 0.3, 0.5 Kgf) for dwell time of 5 s using micro hardness tester. The sharp decrease in the hardness with the increase of load suggests the formation of thin modified surface layer. The observed data reveals that hardness increases with increasing nitriding time which may be due to the increase of more nitrogen content in surface layer [5, 15]. Significant increase in hardness (410 HV) is obtained at 2 mbar filling pressure of nitrogen for 14 h of processing time for the imposed load of 0.01 Kgf compared with the hardness (260 HV) of untreated sample.

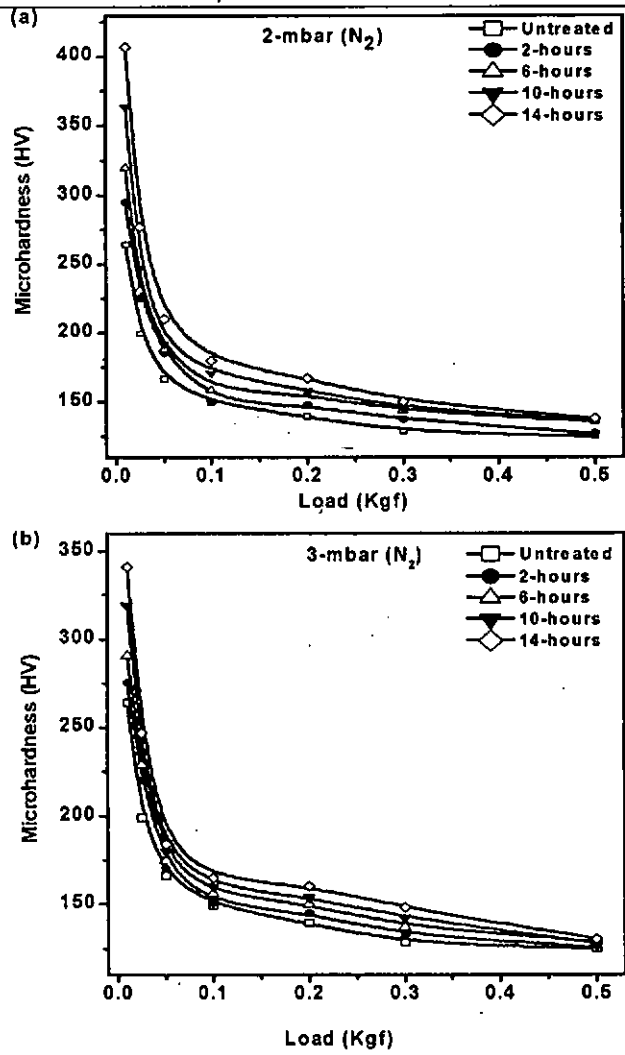

Fig. 11: Variation of surface micro hardness as a function of imposed load for different durations at (a) 2 mbar pressure (b) 3 mbar pressure.

4. CONCLUSIONS

The plasma parameters are measured using Langmuir probe and are decreased with the increase of filling pressure. From the XRD spectra, calculated parameters of nitrided samples treated at 2 mbar and 3 mbar pressures confirm the formation of α_N-Ti and TiN phases. These phases are observed owing to the nitrogen incorporation into titanium matrix as an interstitial solid solution. Modified surface layer thickness and the surface hardness are enhanced for different time durations of 2, 6, 10, and 14 h at 2 mbar pressure whereas decreases at 3 mbar pressure compared with untreated sample. Significant increase in the surface layer thickness and hardness is obtained, when samples are nitrided at 2 mbar filling pressure for 14 h of processing time. It is

observed that 2 mbar pressure is more favorable for infusion of nitrogen in titanium matrix.

REFERENCES

1. C. Alves Jr., C. L. B. Guerra Neto, G. H. S. Morais, C. F. da Silva, V. Hajek, Surf. Coat. Technol., 194 (2000) 196.
2. A. Zhecheva, W. Sha, S. Malinov, A. Long, Surf. Coat. Technol., 200 (2005) 2192.
3. Z. Y. Fan, N. Newman, Appl. Phys. Lett., 73 (1998) 456.
4. M. Shoaib Shah, R. Ahmad, M. Zakaullah, G. Murtaza, Plasma Devic. and Oper., 16 (4) (2008) 247.
5. M. Shoaib Shah, Murtaza Saleem, R. Ahmad, M. Zakaullah, A.Qayyum, G. Murtaza, J. Mat. Process. Technol., 199 (2008) 363.
6. S. Komiya, Materials Science Society Japan, Shokabo, Tokyo, in Japanese, in: Nakamura (Ed.) T. (1996).
7. Nasrullah Khan, M. Shoaib Shah, R. Ahmad, Plasma Sci. Technol., 12 (4) (2010) 452.
8. A. Qayyum, M. A. Naveed, S. Zeb, G. Murtaza, M. Zakaullah. Plasma sci. Technol., 9 (4) (2007) 463.
9. M. Nisha, K. J. Saji, R. S. Ajimsha, N. V. Joshy, M. K. Jayaraj, J. Appl. Phys., 99 (2006) 033304-1.
10. A. Qayyum, M. Ikram, M. Zakaullah, A. Waheed, G. Murtaza, R. Ahmad, A. Majeed, N. A. D Khataak, K. Mansoor, K. A. Chaudhry, J. Mod. Phys., B 17 (2003) 2749.
11. A. Grill, Cold plasma in materials fabrication. IEEE press, New York, (1993).
12. M. J. Druyvesteyn, Der Niedervoltbogen, Z. phys., 64 (1930) 781.
13. S. Miyamoto, F. Kanayama, T. Mune, H. Horiike, Nucl. Fusion, 46 (2006) S313.
14. A. H. Sidney, Introduction to Physical Metallurgy, 2nd Edition, McGraw-Hill, New Delhi. (1997).
15. H.-J. Spies, B. Reinhold, J. Naumann, K. Wilsdorf, Surf. Eng., 17 (1) (2001) 41.
16. E. Badawi, M. A. Abdel-Rahman, S. A. Mahmoud, A.A. Ramadan, Turk. J. phys., 24 (2000) 543.
17. S. Ohira, K. Hiei, M. Iwaki, Nucl. Instrum. Method Phys. Research, B32 (1988) 66.
18. H. Singh, B. Graves David, J. Appl. Phys., 87(9) (2000) 4098.
19. M. M. Turner, R. A. Doyle, M. B. Hopkins, Appl. Phys. Lett., 62 (1993) 3247.

20. A. R. Gonzalez-Elipe, F. Yubero, J. M. Sanz, Low-Energy Ion Assisted Film Growth, Imperial College Press, London, (2003).

21. M. P. Kapczinski, Kinast E. J., dos Santos C. A., J. Phys. D: Appl. Phys., 36 (2003) 1858.

22. S. V. Bagul, S. D. Chavhan, Sharma Ramphal, J. Phys. and Chem. of Solids, 68 (2007) 1623.

23. C. H. Chen, J. M. Yeh, J. Hwang, Nucl. Instr. and Methods of Phys. Research B, 237 (2005) 290.

24. M. Moradshahi, T. Tavakoli, S. Amiri, Sh. Shayeganmchr, Surf. Coat. Technol., 201 (2006) 567.

25. Y. Sun, J. Alloys and Comp., 351 (2003) 241.

26. R. S. Rawat, W. M. Chew, P. Lee, T. White, S. Lee, Surf. Coat. Technol., 173 (2003) 276.